

UNIVERSITY OF PAVIA
DEPARTMENT OF PHYSICS

M.SCI. PROGRAMME IN PHYSICAL SCIENCES

**Neutron activation and dosimetry studies
for the design of an accelerator-based
BNCT clinical facility at CNAO**

Master Thesis of
CHIARA MAGNI

Supervisor
PROF. SILVA BORTOLUSSI

Co-supervisors
DR. IAN POSTUMA
DR. MICHELE FERRARINI

Academic Year 2016/2017

Contents

1	Introduction	1
2	Aluminum fluoride	5
2.1	Preliminary studies	6
2.2	Neutron activation analysis	7
2.2.1	Short-lived isotopes	8
2.2.2	Long-lived isotopes	12
2.2.3	Traces quantification	13
2.2.4	Results and future studies	15
2.3	Activation of BSA	19
2.3.1	Results	23
3	Air activation in treatment room	27
3.1	Simulations	27
3.2	Results	29
4	Patient and air dosimetry	33
4.1	Air dosimetry	33
4.1.1	Equivalent dose	34
4.1.2	Ambient dose equivalent	35
4.1.3	Results	36
4.2	Patient dosimetry	45
4.2.1	Results	46
5	Activation of walls and patient	49
5.1	Walls activation	49
5.1.1	Results	50
5.2	Patient activation	58
5.2.1	Urine activation	58
5.2.2	Body activation	59
	Conclusions and future studies	63
	Bibliography	65

Chapter 1

Introduction

Boron Neutron Capture Therapy (BNCT) is an experimental form of radiotherapy for the treatment of malignant tumors, based on tissues enrichment with the stable isotope boron-10 and on successive irradiation with low energy neutrons [1]. The capture of a thermal neutron in boron, with cross section much greater compared to other elements present in biological tissue, produces two high-LET particles through the reaction $^{10}\text{B}(n,\alpha)^7\text{Li}$. These particles lose their energy in a path of the order of $10\ \mu\text{m}$, comparable with a cellular diameter, and cause irreversible damages to the DNA. Provided a higher ^{10}B uptake by carcinogenic cells with respect to normal ones, the overall effect of the irradiation is the lethal damage of tumour while sparing the surrounding healthy tissues. This selective effect is a promising feature in the field of cancer therapy and makes BNCT a potential therapeutic option for disseminated, infiltrated or non-operable tumors.

The typical sources of neutrons for BNCT are nuclear reactors. Nevertheless, at the present time, BNCT research is moving towards facilities based on accelerators, which are more convenient to use inside an health care environment. Indeed, reactors present characteristics that make them difficult to employ for medical use: complex installation, maintenance and operation, security issues, difficulties in obtaining the necessary political and social support.

Neutrons can be obtained from protons or deuterons accelerators through the reactions (p,n) or (d,n) on targets of beryllium or lithium [2]. The optimal beam for BNCT depends on the position of the malignancy to be treated: for shallow tumours thermal neutrons are needed, while for deep-seated tumours epithermal neutron beams are used: they thermalize in the first layers of tissues and arrive at the tumour target with the suitable energy. Neutrons from accelerators present an harder spectrum with respect to the one needed for BNCT. In order to obtain the optimal beam for the treatment, a Beam Shaping Assembly (BSA) is used, i.e. an ensemble of materials to shape, collimate and moderate the beam.

The Italian National Institute of Nuclear Physics (INFN) in the framework of the project Multidisciplinary Neutron Source (MUNES), designed and manufactured a Radio Frequency Quadrupole (RFQ) proton accelerator, capable to deliver 5 MeV protons with 30 mA current in a Continuous Wave (CW) mode. This accelerator, coupled with a beryllium target, can produce a high neutron flux through the reaction $^9\text{Be}(p,n)^9\text{B}$, and with an appropriate BSA it can be used to provide a neutron

beam suitable for BNCT treatments [3].

A project to install the INFN RFQ in Pavia to build a BNCT clinical facility is under design. The BNCT facility is part of the expansion of the *Centro Nazionale di Adroterapia Oncologica* (CNAO¹), which would thus become the first in the world offering two types of hadron therapy (protons and carbon ions) and BNCT.

This thesis investigates some radiation protection aspects to be taken into account for the design of the BNCT clinical facility at CNAO *Phase II*.

Different compositions and geometries of BSA have been designed and tested in order to determine the best configuration capable to achieve a neutron spectrum able to deliver an advantageous dose distribution in real cases of deep-seated tumours located in the limbs [4] and in the torax [5]. The optimal energy range was proved to be between 1 and 10 keV. To tailor the beam, a number of materials with suitable cross sections have been simulated as the components of the BSA. The obtained beams were evaluated according to the required physical characteristics (epithermal flux, level of contaminations) and on the basis of the dose delivered to tumour while keeping the dose to normal tissues below the tolerance limits. The optimal beam was then selected by choice of the most performing treatment planning simulations [6].

Aluminum fluoride (AlF₃) resulted the most performing material for the BSA. This material reduces the fast component of the ⁹Be(p,n)⁹B reaction without shifting the energy spectrum to the thermal range. AlF₃ allows a very low fast neutron contamination ($< 10^{-12}$ Gy cm² after 30 cm of moderation) and an epithermal flux at the beam port greater than 10⁹ cm⁻² s⁻¹.

AlF₃ in solid form is a new material obtained by powder sintering at the Department of Chemistry of University of Pavia in collaboration with INFN, and it is now being tested in its mechanical characteristics before and after irradiation. To experimentally study AlF₃, powder of different purities and provenance have been analyzed, before and after sintering process. In particular, the presence of traces of elements different than Al and F could lead to radiation protection issues because of neutron activation. Neutron activation is the process in which neutron irradiation induces radioactivity in materials, and occurs when atomic nuclei capture free neutrons, becoming heavier and entering excited states. This process may result in the formation of unstable activation products, with half-lives ranging from small fractions of second to many years. Neutron activation analysis is a very sensitive and accurate method of trace element analysis, based on sample irradiation with neutrons, which cause the elements to form radioactive isotopes. Since the radioactive emissions and radioactive decay paths are well known for each element, it is possible to determine the isotopic composition of the material investigated by studying the spectra of the emissions from the activated sample.

We have performed neutron activation analysis on samples of two different types of AlF₃ powder, in order to determine their composition and evaluate the radiation

¹<http://www.cnao.it>

protection issues related to their use in the clinical facility. The results of this first part lead to a complete characterization of AlF_3 in its isotopic composition and neutron activation aspects, and allow the choice of the most convenient kind of powder to use in the BSA.

Once established the BSA composition, the second part of the work focuses on the design of the treatment room. The effects of neutron irradiation in the environment have been studied by Monte Carlo simulations, with MCNP6 code [7]. MCNP, Monte Carlo N-Particle, is a transport code that simulates nuclear interactions of neutrons with matter on a wide energy range and it is the most used simulation code in BNCT. We have used the version MCNP6, an evolution of the previous MCNP5 and MCNPX, to run simulations of a clinical irradiation in a BNCT clinical facility based on RFQ proton accelerator (5 MeV, 30 mA). Initially, particular attention has been devoted to the activation of air in the treatment room: neutron irradiation of air produces the radioactive isotope argon 41, through the reaction $^{40}\text{Ar}(n,\gamma)^{41}\text{Ar}$. According to the design goal in use at CNAO, the air specific activity released in the environment must not exceed 1 Bq/g, thus the effect of different materials composing walls has been assessed in order not to overcome this value.

Once ensured compliance with this constraint, dosimetry studies have been performed. Equivalent dose-rate distribution in the room has been evaluated, along with the dose absorbed by the principal organs of an anthropomorphic model. Another aspect analyzed in this work is the residual activity, i.e. the radioactivity present due to neutron activation after a certain number of hours of irradiation, both in the patient body and in the materials present in the treatment room.

The results of this work represent a preliminary evaluation of the radiation protection issues that are connected with the construction of a BNCT treatment room. They allow the selection of materials to be used for the walls and in the BSA, thus representing an important ensemble of prescriptions to guide the design of the building. With the described calculation it has been demonstrated that a clinical facility based on a 5 MeV 30 mA RFQ coupled with a Be target is feasible from the point of view of the compliance with radiation protection regulation.

Chapter 2

Aluminum fluoride

As anticipated in the Introduction, aluminum fluoride (AlF_3) has been proved to be the most effective material to tailor an epithermal beam for BNCT of deep seated tumours, starting from the neutrons produced in the Be target by 5 MeV protons. Powder is not suitable to this end, because its density is low even if pressed (reaching 1/3 of nominal density) and its uniformity in the entire geometry could not be guaranteed. For this reason, to obtain the best performance, AlF_3 must be made solid through sintering process. The new material has to be characterized by: high and uniform density (as close as possible to the nominal one) and sufficient mechanical resistance. Therefore a solid material is needed, and it was obtained by the sintering of its powders.

We purchased two kinds of AlF_3 powder, a chemical grade powder ("pure", origin: VWR, supplier *Alpha Aesar*, with declared purity > 99.99% in metals) and an industrial one ("raw", from *Fluorsid*, Cagliari). While some samples of these powders have been subjected to sintering process at the Chemistry Department of University of Pavia, others have been tested through neutron activation analysis. The goal was to verify the isotopic composition of the powders, identifying the impurities present and evaluating radioprotection aspects related to their use in the BSA. The most important element from the point of view of activation is of course aluminum, due to its high percentage in the material. In addition to Al, whose half-life is short (2.2414 minutes), some impurities may constitute a problem in the long term if activated.

To perform neutron activation analysis of aluminum fluoride powders, the samples, weighed with a precision of 0.01 mg, have been inserted into suitable plastic containers made of polyethylene, and activated through irradiation in the reactor *Triga Mark II* at L.E.N.A. of University of Pavia. In Figure 2.1 the various specimens of AlF_3 powder analyzed are shown. The spectra of the activated material have been acquired with the HPGe detector of Radiochemistry laboratory at L.E.N.A., and then analyzed with the software *GammaVision*¹. This software allows calibration in intrinsic and geometric efficiency, and, by comparing the energies of the experimental peaks with a library of emissions associated to nuclides, it is possible to trace the radioisotopes present in the samples. Furthermore, *GammaVision* returns, for each peak, the corresponding nuclide activity through the number of counts, i.e. the peak

¹EG&G ORTEC, *GammaVision* software, version 5.10



Figure 2.1: Irradiated samples of aluminum fluoride powders

area.

2.1 Preliminary studies

A preliminary assessment of the samples activation was necessary to set-up the procedure for a more detailed analysis. Two samples have been irradiated for 3 hours in the Central Thimble (CT) of the reactor at maximum power (250 kW), thus subjected to a neutronic flux of $5.9 \times 10^{12} \text{ cm}^{-2} \text{ s}^{-1}$. The samples irradiated in this first measurement were:

- Sample 1: 40.97 mg of raw AlF_3
- Sample 5: 98.59 mg of pure AlF_3

Spectra were acquired with the Ge detector at about 24, 72 and 400 hours from irradiation. Figure 2.2 shows an example of spectrum obtained. Spectra have been analyzed with *GammaVision* to draw up an initial list of isotopes present in AlF_3 samples.

We have also used a tissue-equivalent detector, the scintillation plastic dosimeter *AtomTex* model No. AT1121, to measure the contact dose of the samples, shown as a function of time in Figure 2.3. It can be noted that the raw sample presents a dose rate about 5 to 6 times higher than that of the pure one. This is a result we expected, from the declared purity of the samples analyzed: 90% for the *Fluorsid* powder (raw) and 99.9% for the *Alpha Aesar* one (pure).

This dose measurements allowed setting the irradiation time for the next measurements, performed in order to evaluate the isotopic composition, the dose-rate and activity time evolution of the samples.

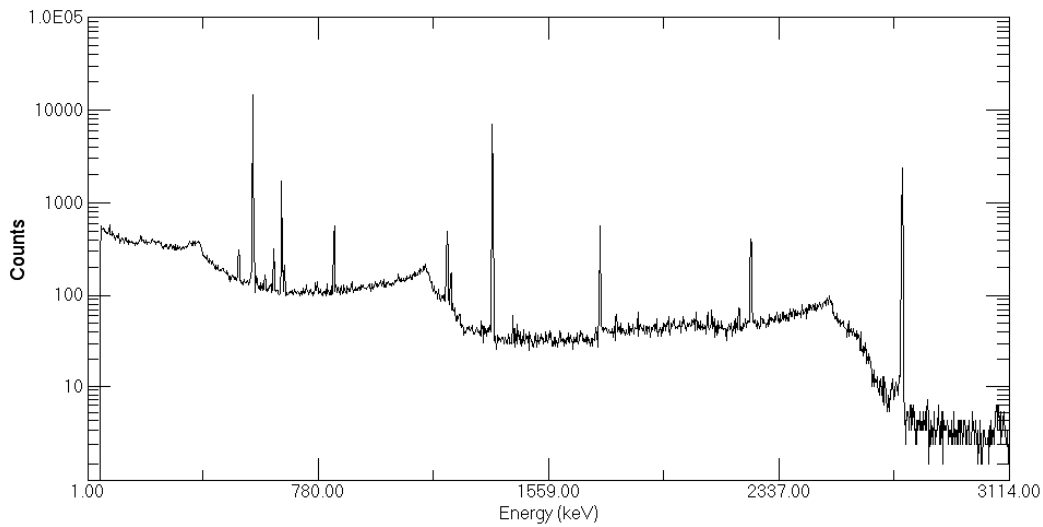


Figure 2.2: Spectrum of an activated sample of raw powder

2.2 Neutron activation analysis

The preliminary analysis showed that an irradiation of the order of 1 hour in the CT was enough to point out the desired impurities and that samples were handleable after some hours. The detailed analysis had two main goals: to establish the mass content of Al and Na, and to point out other impurities.

Aluminum is of course the main component of the BSA that is activated during irradiation, through the reaction $^{27}\text{Al}(n,\gamma)^{28}\text{Al}$ with thermal cross section² of 0.235 barn ([8], [9]). Sodium is another element whose neutron activation is relevant, producing the radioisotope Na-24 with half-life of 14.9590 hours. In addition to the Na present in the powder, which activates following the reaction $^{23}\text{Na}(n,\gamma)^{24}\text{Na}$ (thermal cross section 0.53 barn [8], [9]), also the irradiation of aluminum produces sodium 24, through $^{27}\text{Al}(n,\alpha)^{24}\text{Na}$ (cross section shown in Fig. 2.4).

To measure the mass percentages of Al and Na in the powders, samples of AlF_3 were irradiated together with two standards, one of sodium and one of aluminum, i.e. samples with known amount of Al and Na. The comparison between the activation of the standards and the one of the powders allows the determination of aluminum and sodium mass in AlF_3 . The Na standard is a liquid solution, NaCl with sodium in concentration of 204.5 ppm³, while Al standard is a thin round foil (5 mm of diameter, 0.2 mm thick) of metallic Au-Al with aluminum purity 99.953% (Figure 2.5).

For the other impurities present in AlF_3 powders we do not have standards, thus the quantification must be obtained from the emission peaks. The neutron spectrum in the CT is harder than the one to which the BSA will be subjected, thus not all the peaks are of real interest. Specifically, only the isotopes with an activation threshold

²Cross section at neutron energy equal to 0.025 eV.

³The term ppm stands for *parts per million*, meaning the presence of 204.5 μg of sodium per gram of solution.

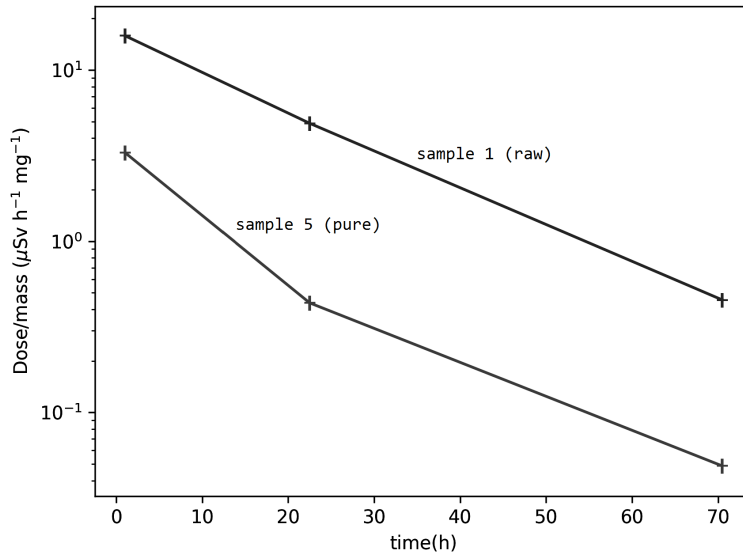


Figure 2.3: Contact dose of AlF_3 samples as a function of time

of less than 3.5 MeV were considered. Among these, only those obtained with reactions whose cross section are proportional to $1/v$ can be quantified by activation analysis method.

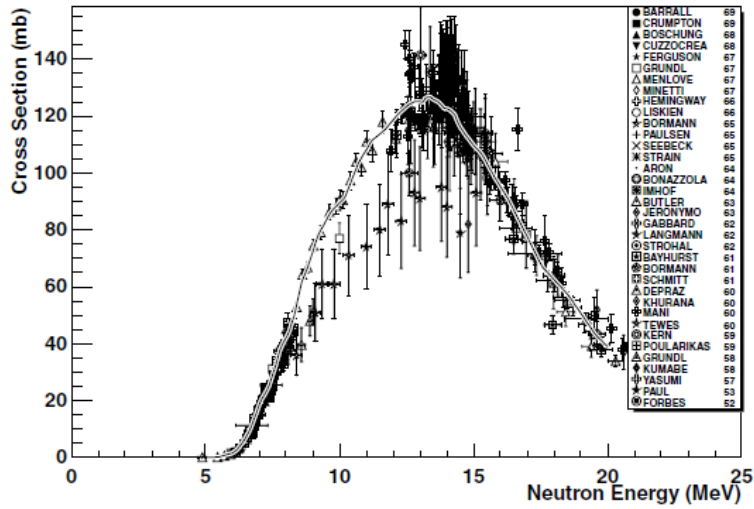
Table 2.1 summarizes the samples prepared, the irradiation times and positions in the reactor. The irradiation in the Central Thimble (CT) lasted 1 hour, while the irradiation in the Rabbit Channel lasted 30 seconds.

Sample	Description	Composition	Mass [mg]	Irradiation
1	raw Aluminum Fluoride	AlF_3	40.97	CT 1 h
5	pure Aluminum Fluoride	AlF_3	42.50	CT 1 h
4	raw Aluminum Fluoride	AlF_3	98.59	Rabbit 30 s
6	pure Aluminum Fluoride	AlF_3	76.87	Rabbit 30 s
TER	Na std (Na: 204.5 ppm)	NaCl	295.0	Rabbit 30 s
C1	Al std (Al purity: 99.953%)	Au-Al	7.5	Rabbit 30 s

Table 2.1: Samples and standards irradiated

2.2.1 Short-lived isotopes

Rabbit System is a pneumatic transfer system that allows to convey very rapidly a specimen capsule to the reactor core and back, therefore it is used for the production of very short-lived radioisotopes [10]. Table 2.2 lists the irradiations performed in the Rabbit System. The spectra of these activated samples have been acquired, first immediately after irradiations to trace isotopes with about 1 minute half-lives, and

Figure 2.4: Cross section of reaction $^{27}\text{Al}(n,\alpha)^{24}\text{Na}$

Sample	Description	Start	Stop
4	raw AlF_3	15:19:07	15:19:37
6	pure AlF_3	15:27:22	15:27:52
TER	Na std	15:30:31	15:31:01
C1	Al std	15:31:20	15:31:50

Table 2.2: Irradiations performed with Rabbit

then about 20 minutes later, in order to point out isotopes with longer lives.

The isotopes traced by gamma spectroscopy through *GammaVision* are listed in Table 2.3, along with the samples in which they have been found. Elements common to raw and pure samples of aluminum fluoride are Al-28, Mg-27 and Na-24. Only in raw AlF_3 we find As-76, Co-60 and Ga-72, only in pure AlF_3 Cl-38 and Sb-124. About long half-life isotopes, in raw AlF_3 is present Co-60 with $T_{1/2}=5.2714$ years, while in pure AlF_3 Sb-124 with $T_{1/2}=60.20$ days.

Al and Na percentages

Starting from the spectra of activated samples the weight percentage of sodium and aluminum in the AlF_3 powders was determined.

The quantity of interest for the weight percentages determination is the mass m of the element in question, which is related to the total number N of interaction centers in the irradiated volume, through the atomic weight of the isotope A and the Avogadro constant N_A :

$$N = \frac{m}{A} N_A \quad (2.1)$$



Figure 2.5: Standards used (left:Al, right:Na)

Nuclide	Half-Life	Present in samples			
		raw	pure		
Al-28	2.414 min	raw	pure		Al std
As-76	1.0778 d	raw			
Au-198	2.69517 d				Al std
Cl-38	37.24 min		pure	Na std	
Co-60	5.2714 y	raw			
Ga-72	14.10 h	raw			
Mg-27	9.458 min	raw	pure		Al std
Mn-56	2.5785 h				Al std
Na-24	14.9590 h	raw	pure	Na std	Al std
Sb-124	60.20 d		pure		

Table 2.3: Nuclides found in samples irradiated with rabbit

This value, multiplied by the neutron flux ϕ and by the cross section σ of the reaction involved, both at a certain neutron energy E , is equal to the number of reactions per unit time, called "reaction rate", R :

$$R = \phi\sigma N \quad (2.2)$$

This quantity accounts for the creation of the radioisotopes, but we must consider that at the same time they may decay. Thus, balancing with the nuclei that decay and indicating with λ the decay constant, the time evolution of activated nuclei N_{act} is overall given by:

$$\frac{dN_{act}}{dt} = R - \lambda N_{act} \quad (2.3)$$

from which the number of activated nuclei at the end of irradiation results to be:

$$N_{act} = \frac{R}{\lambda}(1 - e^{-\lambda t_{irr}}) \quad (2.4)$$

where t_{irr} represents the irradiation time.

The number of activated nuclei is estimated from the number of counts ΔN which the software *GammaVision* returns as the integral of a peak. This value represents the variation of radioactive nuclei in the interval between the start (t_1) and the stop (t_2) of the spectrum acquisition, thus:

$$N_{act} = \frac{\Delta N}{(e^{-\lambda t_1} - e^{-\lambda t_2})} \cdot \frac{1}{\epsilon} \cdot \frac{1}{BR} \quad (2.5)$$

where we have taken into account the efficiency ϵ with which *GammaVision* detects photons at the energy of considered peak, and the Branching Ratio of the emission to which the peak is related. Hence the reaction rate is finally equal to:

$$R = \frac{\lambda N_{act}}{(1 - e^{-\lambda t_{irr}})} = \frac{\lambda}{(1 - e^{-\lambda t_{irr}})} \cdot \frac{\Delta N}{(e^{-\lambda t_1} - e^{-\lambda t_2})} \cdot \frac{1}{\epsilon} \cdot \frac{1}{BR} \quad (2.6)$$

Once calculated R , Eq. 2.2 can be used to determine N , known the neutron flux and the cross section of the reaction involved.

Nevertheless, in our case, Eq 2.2 is not straightforward, since the neutron flux is not monoenergetic and also the cross section depends on the neutron energy E . The relation to use would be, integrating over the energy spectrum:

$$R = N \int_{E_{min}}^{E_{max}} \phi(E)\sigma(E)dE \quad (2.7)$$

For this reason, the quantification is obtained by comparison with the activation of the standards, for which the number of activation centers is known. Considering the same reaction (thus the same cross section) and if the standard and the sample of unknown composition are irradiated with the same flux, we can equal $\phi\sigma$ from Eq. 2.2, obtaining:

$$N_{sample} = N_{STD} \frac{R_{sample}}{R_{STD}} \quad (2.8)$$

where N_{STD} and R_{STD} are the number of interaction centers and the reaction rate of the standard, and N_{sample} and R_{sample} the analogous quantities for the sample investigated. The reaction rate are evaluated through Eq. 2.6 from the peaks of the analyzed spectra.

The reactions under study are:

- $^{27}\text{Al}(n,\gamma)^{28}\text{Al}$
- $^{27}\text{Al}(n,\alpha)^{24}\text{Na}$
- $^{23}\text{Na}(n,\gamma)^{24}\text{Na}$

The mass percentages obtained applying the described method are listed in Table 2.4. Values obtained for aluminum are in agreement with what was expected from stoichiometric calculations (about 32%).

Samples	Mass percentages	
	Na	Al
raw AlF_3	0.06%	29.4%
pure AlF_3	0.0012%	26.8%

Table 2.4: Mass percentages obtained in AlF_3 samples

2.2.2 Long-lived isotopes

The CT is the channel located at the center of the core, providing space for irradiation of samples at the point of maximum flux, and it has been used for radioisotopes with longer lives [10].

Since, in preliminary study, with samples irradiated in CT for 3 hours we had obtained a contact dose of 1 mSv/h at the extraction, we have decided to reduce irradiation time to 1 hour. The two samples were inserted together in CT at 14:53 on April 3rd and irradiated for 1 hour at maximum power, then the analysis was started after a cooling of about 24 hours (Table 2.5). At the extraction, the sample that was more active was the raw one.

Sample	Description	Start	Stop
1	raw AlF_3	14:53:30	15:53:30
5	pure AlF_3	14:53:30	15:53:30

Table 2.5: Irradiations performed in CT

Over about 2 weeks we acquired the spectra of the activated samples, and their analysis has led to the identification of the isotopes listed in Table 2.6.

Dose measurements

The time evolution of the dose due to the activated AlF_3 was reconstructed over a period of about 2 weeks.

Using the scintillation plastic tissue-equivalent dosimeter *AtomTex* model No. AT1121, the dose values at 5, 10, 15 and 30 cm away from each sample were measured. The experimental set-up adopted is shown in Figure 2.6. For each data set, the radiation background present at the time of measurement was also recorded and then subtracted from the dose values returned by the dosimeter.

Figure 2.7 shows the dose as a function of the time at 5 cm from the samples. Although the dose of the raw sample is initially the highest, the situation is reversed after about 240 hours. This is most probably due to the higher content in pure AlF_3 of isotopes which produce, through neutron activation, radionuclides with a long half-life, as shown in Table 2.8.

Nuclide	Half-Life	Present in samples	
As-76	1.0778 d	raw	
Br-82	35.30 h	raw	pure
Co-60	5.2714 y	raw	pure
Cr-51	27.7025 d		pure
Fe-59	44.503 d	raw	
Ga-72	14.10 h	raw	pure
La-140	1.6781 d		pure
Na-24	14.9590 h	raw	pure
Sb-122	2.7238 d	raw	pure
Sb-124	60.20 d	raw	pure
Sc-46	83.79 d	raw	pure
Se-75	119.779 d		pure
Zn-65	244.26 d	raw	

Table 2.6: Nuclides found in samples irradiated in CT

Specific activity

A study about specific activity in function of time was also carried out. The activity has been calculated from the peaks of the spectra collected, choosing for every nuclide the activity of the peak with the maximum number of counts. The error associated depends on the errors on activities given by the software, neglecting the error on the samples mass. Specific activities obtained are represented in function of time in the Figures 2.8 -2.18.

Specific activity values have been fitted⁴ with an exponential decay to estimate the half-life from their time trend, in order to have further confirmation of the identified isotopes. In Table 2.7 a comparison between the half-lives obtained through the fit and the theoretical ones (source: *Radiation Decay* software⁵) is shown. Except for the nuclides for which we have a low number of data, experimental half-lives are in quite good agreement with the theoretical ones.

2.2.3 Traces quantification

Without standards, the quantification of trace elements must be obtained through the determination of the number of interaction centers from Eq. 2.2, using the thermal flux and the cross section at 0.025 eV. It must be taken into account that our experimental analysis has studied AlF₃ activation through irradiation in the reactor, in which, as anticipated, the spectrum is harder than the one that will be present in BSA. We can now focus on non-threshold reactions, the ones that will occur also in the clinical irradiation.

⁴using the programming language Python

⁵Hacker C., *Radiation Decay* software 4th version, Griffith University, 2005

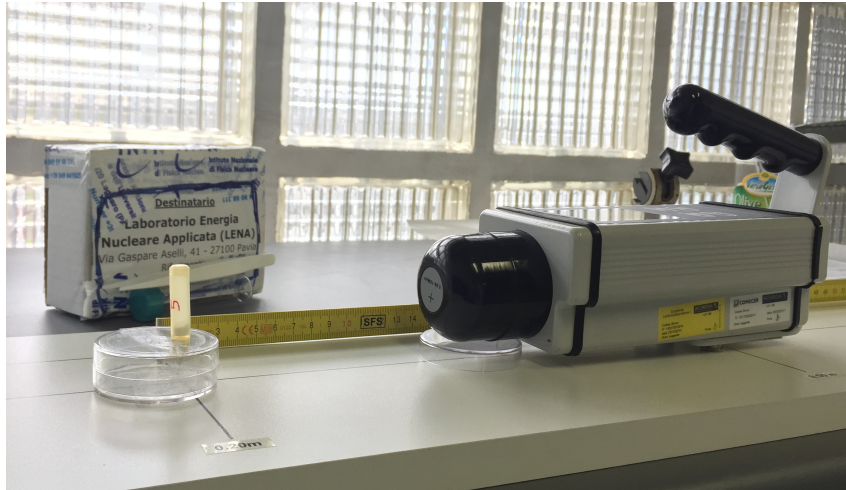


Figure 2.6: Experimental set-up for dose measurements effectuated

Nuclide	Theoretical	Experimental	
		raw	pure
As-76	1.0778 d	(26.3 ± 0.4) h	-
Br-82	35.30 h	(43 ± 5) h	(31.2 ± 0.5) h
Co-60	5.2714 y	(1 ± 7) y	(0.1 ± 0.2) y
Ga-72	14.10 h	(13.7 ± 0.3) h	-
La-140	1.6781 d	-	(3.7 ± 1.8) d
Na-24	14.9590 h	(14.90 ± 0.07) h	(14.5 ± 0.2) h
Sb-122	2.7238 d	-	(2.64 ± 0.04) d
Sb-124	60.20 d	-	(29 ± 5) d

 Table 2.7: Theoretical and experimental half-lives of nuclides found in raw and pure AlF_3

The reactions to be considered are:

- $^{27}Al(n,\gamma)^{28}Al$
- $^{59}Co(n,\gamma)^{60}Co$
- $^{139}La(n,\gamma)^{140}La$
- $^{123}Sb(n,\gamma)^{124}Sb$
- $^{75}As(n,\gamma)^{76}As$
- $^{50}Cr(n,\gamma)^{51}Cr$
- $^{26}Mg(n,\gamma)^{27}Mg$
- $^{45}Sc(n,\gamma)^{46}Sc$
- $^{81}Br(n,\gamma)^{82}Br$
- $^{58}Fe(n,\gamma)^{59}Fe$
- $^{23}Na(n,\gamma)^{24}Na$
- $^{74}Se(n,\gamma)^{75}Se$
- $^{37}Cl(n,\gamma)^{38}Cl$
- $^{71}Ga(n,\gamma)^{72}Ga$
- $^{121}Sb(n,\gamma)^{122}Sb$
- $^{64}Zn(n,\gamma)^{65}Zn$

For each of the activated isotopes, the mass percentage in raw and pure AlF_3 has been estimated, and obtained values are reported in Table 2.8. The errors have been calculated as the sum of the relative errors of counts, cross sections and fluxes, neglecting the uncertainty on other quantities used for the calculation. The isotopes highlighted in the Table 2.8 are those with activation products having a half-life greater than 10 days. The higher percentage of long-lived isotopes in pure AlF_3 can

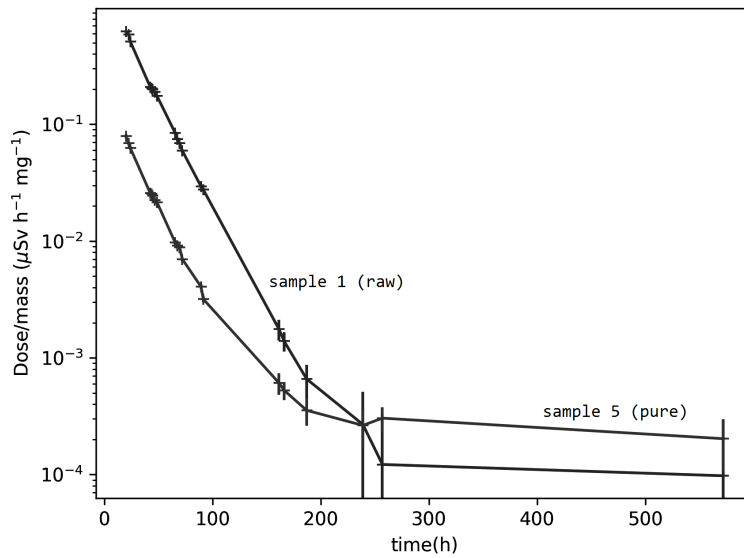


Figure 2.7: Time evolution of AlF_3 samples dose at 5 cm

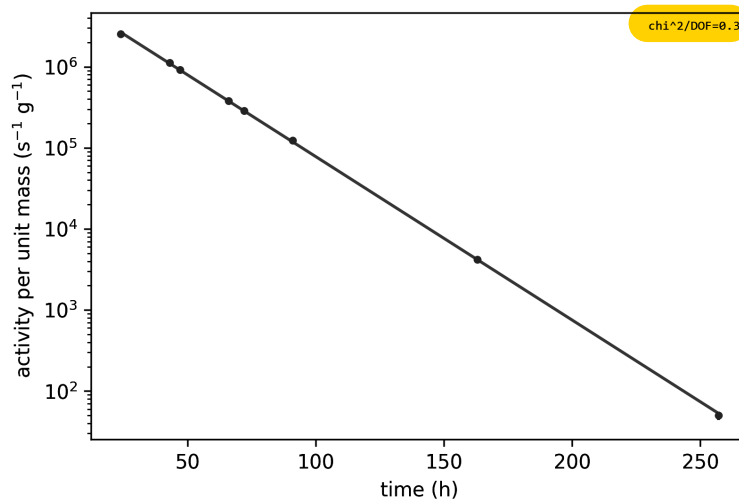


Figure 2.8: Specific activity of Na-24 in sample 1 (raw AlF_3)

explain the dose evolution of the samples, seen in Fig. 2.7.

2.2.4 Results and future studies

Table 2.9 reports an overall summary of the results of these activation studies for the two types of AlF_3 measured.

From these findings it is possible to classify the properties of pure and raw AlF_3 as

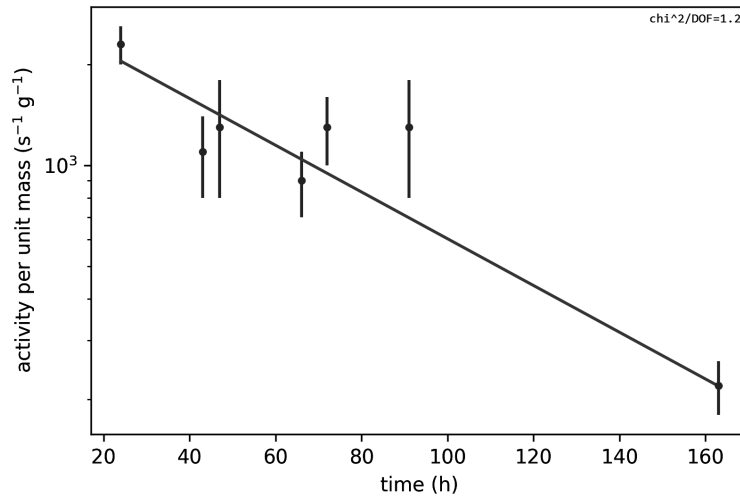


Figure 2.9: Specific activity of Br-82 in sample 1 (raw AlF_3)

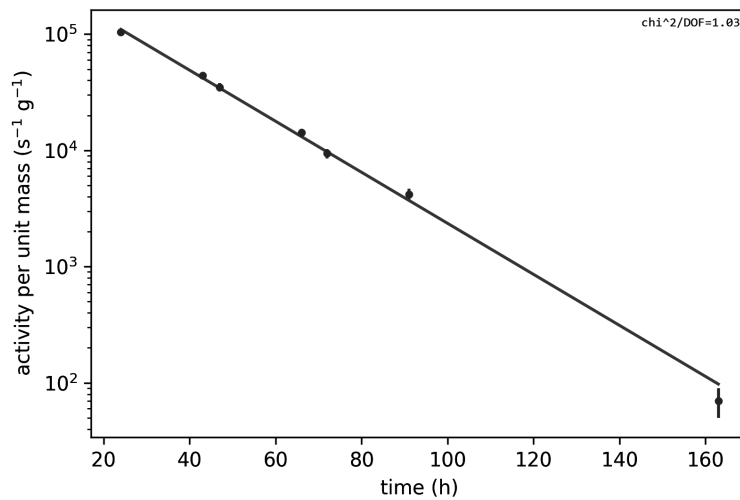


Figure 2.10: Specific activity of Ga-72 in sample 1 (raw AlF_3)

following:

- pure AlF_3 : less dose at the extraction
- raw AlF_3 : more favourable dose decrease as a function of the time after irradiation

The experiments performed with the two powder types concerning the possibility to obtain a solid material with high density demonstrated that raw material is preferable: it gives better results in terms of sintering, reaching in solid form high density values (of about 3 g/cm^3 , while 1.5 g/cm^3 is the maximum value obtained for the

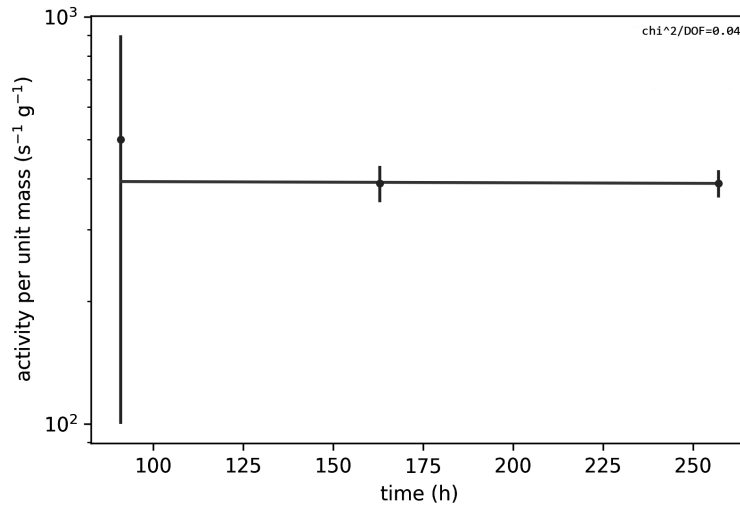


Figure 2.11: Specific activity of Co-60 in sample 1 (raw AlF_3)

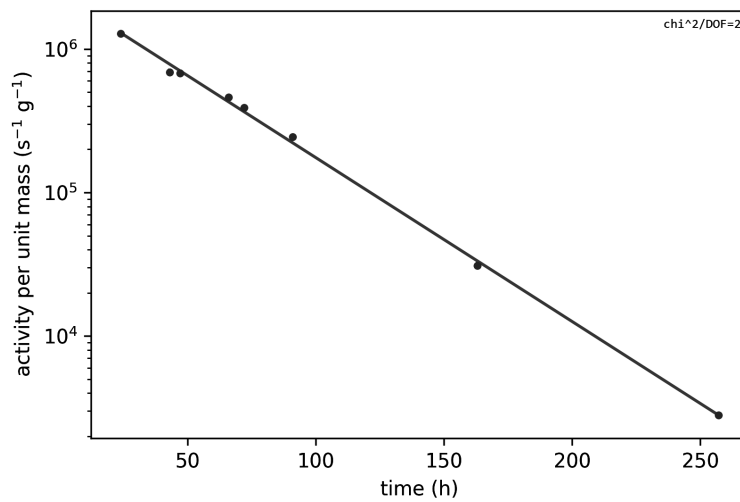


Figure 2.12: Specific activity of As-76 in sample 1 (raw AlF_3)

pure AlF_3). This could be due to the finer granulometry of the raw powder, or to its content of a higher percentage of impurities that may act as a ligand. Also considering that the impurities measured in the raw material do not affect the spectrum optimization of the final beam, aluminum fluoride of industrial grade was thus proven to be a suitable material to build the BSA for a clinical BNCT neutron beam.

Further studies on sintered AlF_3 are planned, in order to verify whether chemical composition and dose characteristics change in the sintering process. Moreover, sintered AlF_3 elements will be irradiated to study the effects of radiation on the

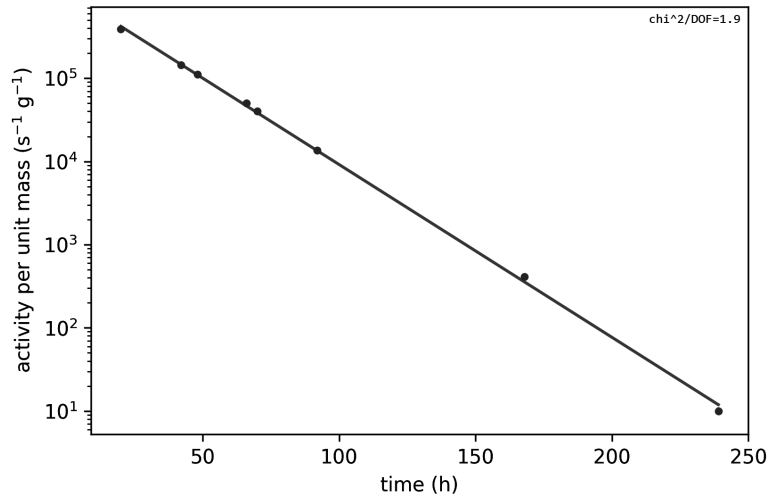


Figure 2.13: Specific activity of Na-24 in sample 5 (pure AlF_3)

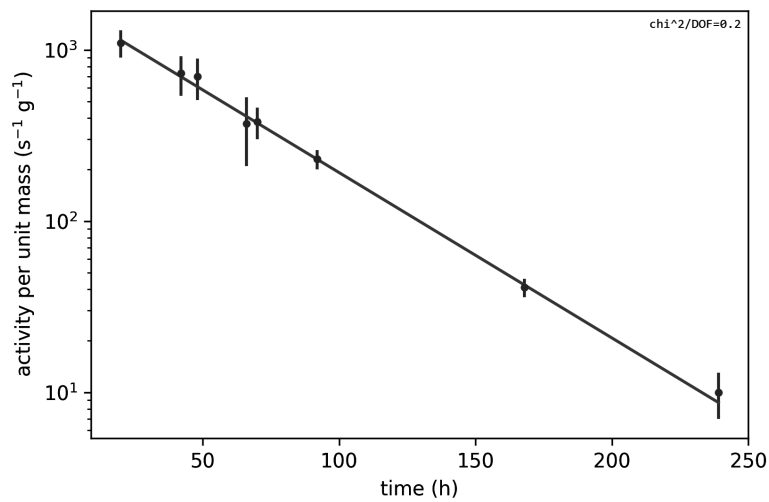


Figure 2.14: Specific activity of Br-82 in sample 5 (pure AlF_3)

mechanical properties of the new material. As a preliminary study, two samples of sintered AlF_3 have been irradiated at L.E.N.A., in the Lazy Susan channel of the reactor [10]. The samples were inserted on July 20th and extracted on July 27th after a total of 20 hours of irradiation at maximum power. Fig. 2.19 shows the two samples irradiated (the tallest cylinder is the pure one). The material appear intact except for some minimal damages on the edges, especially in the pure sample, that, however, was characterized by low density and seemed to show lower resistance to mechanical stress. On September 6th we have measured the contact dose of the samples, resulting comparable with the background. We then acquired two spectra,

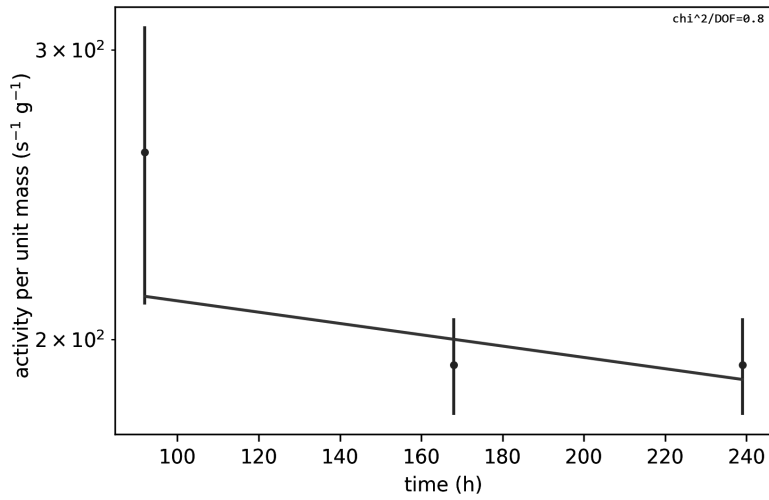


Figure 2.15: Specific activity of Co-60 in sample 5 (pure AlF_3)

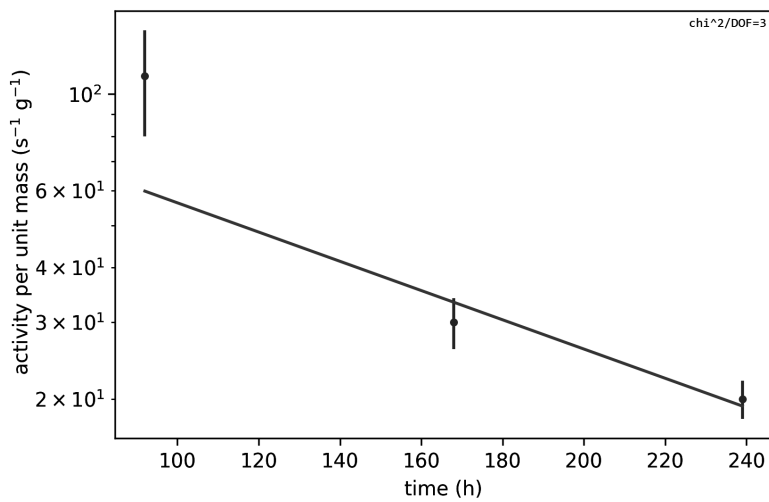


Figure 2.16: Specific activity of La-140 in sample 5 (pure AlF_3)

showing the presence of the long-lived isotopes Co-60, Sb-124 and Zn-65 revealed in the previous experiments. A more detailed analysis will be performed, including mechanical resistance tests on irradiated samples.

2.3 Activation of BSA

Assessed that the industrial powder has the best characteristics in terms of mechanical properties and has acceptable properties from a radioprotection point of view, a study of the neutron activation of the BSA has been performed, simulating the solid

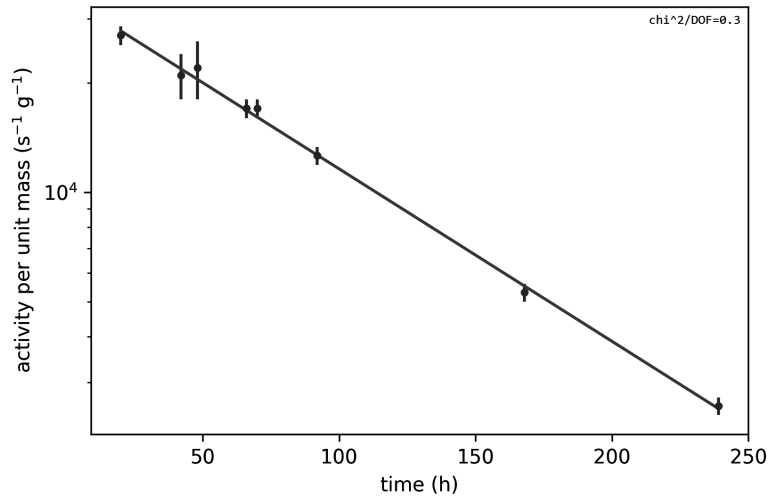


Figure 2.17: Specific activity of Sb-122 in sample 5 (pure AlF_3)

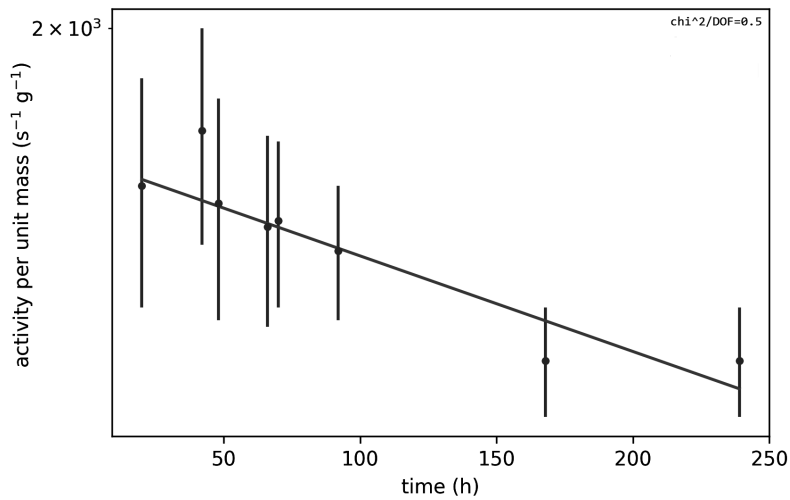


Figure 2.18: Specific activity of Sb-124 in sample 5 (pure AlF_3)

raw AlF_3 assembly. Its residual activity after a certain number of hours of irradiation represents an important effect, both for the patient radioprotection and for any maintenance work to be effectuated on the facility.

The percentages of impurities determined as explained above (and summarized in Table 2.8) was thus introduced into a simulation of the BSA. This calculation gives an estimation of the radiation protection issues that must be considered for the construction of the clinical facility, and it is necessary since the spectrum of neutrons emerging from the accelerator is different that the one in the Central Thimble of

Nuclide	Mass percentages [ppm]	
	raw	pure
As-75	230±5	—
Br-81	1.09±0.12	1.7±0.3
Cl-38	—	8.3±1.3
Co-59	11±1	14±1
Cr-50	—	0.10±0.02
Fe-58	0.48±0.03	—
Ga-71	9.1±0.4	0.18±0.05
La-139	—	0.34±0.07
Mg-27	6300±1100	—
Sb-121	0.39±0.02	40±2
Sb-123	0.46±0.02	69±6
Sc-45	0.022±0.001	0.34±0.01
Se-74	—	0.054±0.004
Zn-65	19±2	—

Table 2.8: Values obtained for mass percentages of impurities in AlF_3 samples

the reactor (Fig. 2.20 shows a comparison of the two neutron spectra). Simulations have been performed using the Monte Carlo code MCNP6, reproducing the geometry of the BSA and running a coupled neutron-photon transport through the geometry. The geometry of the facility is shown in Fig. 2.21, where the AlF_3 has been depicted in grey. The neutron source was defined in the Be target as described in [6], taking into account the experimental double differential spectrum emerging from the (p,n) reaction in Be at 5 MeV [11].

The residual activity can be determined from the number of unstable isotopes created by the activation, for which the reaction rate is needed. Reaction rates are obtainable in MCNP through simulations scoring the neutron flux, i.e. with a F4-type tally, combined with a tally modifier that indicates the nuclear reaction of interest and the isotope involved, as follows:

```
F4:n "cell"
FM4 C "material" "reaction"
```

where “cell” refers to the cell in which the reaction takes place, “material” is a material opportunely defined in the simulation input, and made 100% of the reaction target isotope, and “reaction” is a number indicating to MCNP which kind of reaction is occurring. For example, for the reaction $^{27}Al(n,\gamma)^{28}Al$ in a hypothetical cell 3, the syntax used would be the following:

```
m5 13027 1
F4:n 3
FM4 C 5 102
```

Nuclide	Half life	[units]
Al-28	2.414	min
As-76	1.0778	d
Br-82	35.30	h
Cl-38	37.24	min
Co-60	5.2714	y
Cr-51	27.7025	d
Fe-59	44.503	d
Ga-72	14.10	h
Mg-27	9.458	min
Na-24	14.9590	h
Sb-122	2.7238	d
Sb-124	60.20	d
Sc-46	83.79	d
Se-75	119.779	d
Zn-65	244.26	d

Table 2.9: Radioisotopes traced through gamma spectroscopy in the powders (activation products of AlF_3 constituents, see previous Table)

“C” is a multiplicative constant that represents the number of atoms of the isotope present in the cell where the reaction takes place, 5 is the material identifier (atomic number 13 and mass number 027), and 102 refers to (n, γ) cross section tables. C is calculated from the total numbers of atoms of the isotope considered, N , which are present in the cell of the reaction (Eq. 2.1). Known the isotope mass percentage $m\%$ in the cell, and indicating with N_A the Avogadro constant and with A the atomic weight of the isotope, we have:

$$C = \frac{m\% \cdot N_A}{A} \cdot 10^{-24} \cdot I \quad (2.9)$$

where 10^{-24} is the conversion factor from barn to cm^2 , and I the source intensity, in our case $9.6 \cdot 10^{13} s^{-1}$.

In this way, the tally provides the number of reactions per second and per gram. The activation reactions are listed in Table 2.10 with their thermal cross sections ([9]) and the values of normalization constant C for the tally, obtained as explained above.

From the simulated reaction rate, the activity at the end of an irradiation has been evaluated using:

$$A = R (1 - e^{-\lambda t_{irr}}) \quad (2.10)$$

where λ is the decay constant of the radioisotope created by activation and t_{irr} the irradiation time, taken conservatively equal to 2 hours.



Figure 2.19: Samples of sintered AlF_3 after an irradiation of 20 hours

2.3.1 Results

The simulated reaction rates for the activations listed above are reported in Table 2.11, with the specific activities after 2 hours of irradiation calculated through Eq. 2.10. MCNP code was run for a time sufficient to obtain a statistical relative error smaller than 0.1%, ensuring the precision of the simulation. The values listed in Table are associated to an error taking into account the precision with which cross section are known (Table 2.10, 4th column).

As expected, the greatest contribute comes from the activation of aluminum. However, the radioisotope Al-28 has a short half-life of about 2 minutes. Activation products with half-lives longer than 10 days, such as Co-60 ($T_{1/2}=5.2714$ y), Fe-59 ($T_{1/2}=44.503$ d), Sb-124 ($T_{1/2}=60.20$ d), Sc-46 ($T_{1/2}=83.79$ d) and Zn-65 ($T_{1/2}=244.26$ d), give specific activities at the end of irradiation smaller than 1 Bq per gram. To assess the cumulative effect of neutron activation in BSA over several treatments, further studies are needed. In particular, the evaluation of activity created through irradiations should take into account a realistic alternation between beam working and stop.

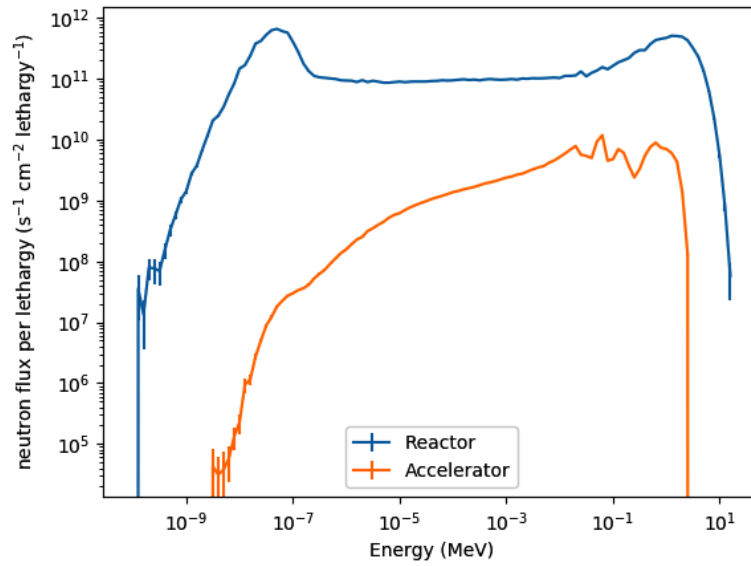


Figure 2.20: Neutron spectra in the BSA and in the reactor

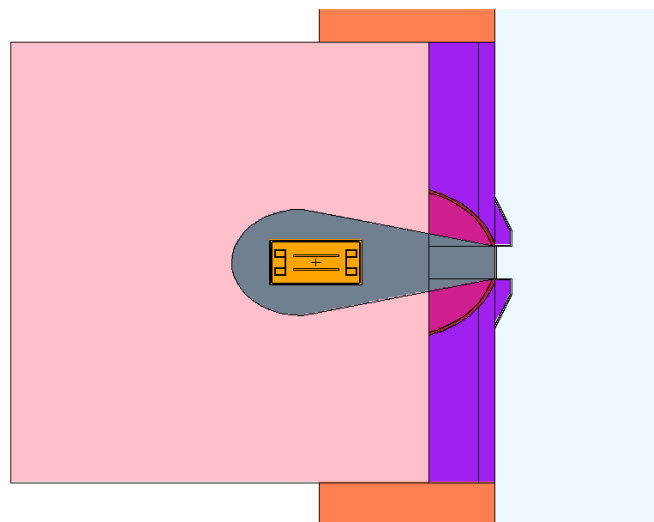


Figure 2.21: MCNP geometry of the facility

Nuclide	Reaction	C	σ [barn]
Al-27	$^{27}\text{Al}(n,\gamma)^{28}\text{Al}$	6.61×10^{11}	0.231 ± 0.003
As-75	$^{75}\text{As}(n,\gamma)^{76}\text{As}$	1.77×10^8	4.23 ± 0.08
Br-81	$^{81}\text{Br}(n,\gamma)^{82}\text{Br}$	7.77×10^5	2.36 ± 0.05
Co-59	$^{59}\text{Co}(n,\gamma)^{60}\text{Co}$	1.12×10^7	37.18 ± 0.06
Fe-58	$^{58}\text{Fe}(n,\gamma)^{59}\text{Fe}$	4.77×10^5	1.30 ± 0.03
Ga-71	$^{71}\text{Ga}(n,\gamma)^{72}\text{Ga}$	7.38×10^6	4.73 ± 0.15
Mg-26	$^{26}\text{Mg}(n,\gamma)^{27}\text{Mg}$	1.41×10^{10}	0.0386 ± 0.006
Na-23	$^{23}\text{Na}(n,\gamma)^{24}\text{Na}$	1.51×10^9	0.530 ± 0.005
Sb-121	$^{121}\text{Sb}(n,\gamma)^{122}\text{Sb}$	1.85×10^5	5.9 ± 0.2
Sb-123	$^{123}\text{Sb}(n,\gamma)^{124}\text{Sb}$	1.71×10^5	1.1 ± 0.1
Sc-45	$^{45}\text{Sc}(n,\gamma)^{46}\text{Sc}$	2.88×10^4	27.2 ± 0.2
Zn-65	$^{64}\text{Zn}(n,\gamma)^{65}\text{Zn}$	1.75×10^7	1.1 ± 0.1

Table 2.10: Activations of BSA constituents and multiplicative constants for their reaction rate tallies

Nuclide	Half-life	R [$\text{s}^{-1} \text{g}^{-1}$]	a [Bq/g]
Al-28	2.414 min	$(2.9 \pm 0.4) \times 10^6$	$(2.9 \pm 0.4) \times 10^6$
As-76	1.0778 d	$(6.05 \pm 0.11) \times 10^5$	$(1.60 \pm 0.03) \times 10^4$
Br-82	35.30 h	$(2.07 \pm 0.04) \times 10^3$	39.02 ± 0.08
Co-60	5.2714 y	$(3.795 \pm 0.006) \times 10^4$	$(5.696 \pm 0.009) \times 10^{-1}$
Fe-59	44.503 d	40.8 ± 0.9	$(2.65 \pm 0.06) \times 10^{-2}$
Ga-72	14.10 h	$(1.31 \pm 0.04) \times 10^4$	$(6.3 \pm 0.2) \times 10^2$
Mg-27	9.458 min	$(8.7 \pm 1.4) \times 10^3$	$(8.6 \pm 1.3) \times 10^3$
Na-24	14.9590 h	$(2.08 \pm 0.02) \times 10^4$	$(9.44 \pm 0.09) \times 10^2$
Sb-122	2.7238 d	$(1.05 \pm 0.04) \times 10^7$	11.0 ± 0.4
Sb-124	60.20 d	$(9.7 \pm 0.9) \times 10^2$	$(4.6 \pm 0.4) \times 10^{-1}$
Sc-46	83.79 d	9.25 ± 0.07	$(3.19 \pm 0.02) \times 10^{-3}$
Zn-65	244.26 d	$(2.3 \pm 0.2) \times 10^3$	$(2.7 \pm 0.2) \times 10^{-1}$

Table 2.11: Simulated reaction rates and specific activities of BSA constituents after 2h of irradiation (in the first column the activation products of reactions listed in previous Table)

Chapter 3

Air activation in treatment room

Another relevant problem in a treatment room where there is a neutron flux of about $10^9 \text{ cm}^{-2} \text{ s}^{-1}$ for irradiation times of the order of 1 hour per patient, is the activation of air. The most important concern regards the activation of argon, through the reaction $^{40}\text{Ar}(n,\gamma)^{41}\text{Ar}$ (thermal cross section 0.7 barn [8], [9]). Argon is a noble gas naturally present in air, in a percentage of about 0.9%. Neutron capture in argon-40 produces the radioactive isotope Ar-41, a beta- emitter with a half life of 109.34 minutes. The fact that argon is a noble gas limits the possibility of filtering it out of the room air, thus, to contain the activity created, the Ar-41 production must be lowered as much as possible.

With this study we have proposed to optimize the materials of the irradiation room to meet a design goal in use at CNAO, according to which the specific activity of air released in the environment must not exceed 1 Bq/g. The CNAO Qualified Expert in Radiological Protection has designed the irradiation room, with different shielding materials and adequate thicknesses to ensure acceptable doses outside. Starting from this project, a geometry of the treatment room has been built with MCNP6 code, as shown in Fig. 3.1. Then, simulations of a clinical irradiation have been run to study the air activation with four different wall compositions:

- ordinary concrete
- concrete + 5% of natural boron (i.e. 1% of ^{10}B)
- ordinary polyethylene
- polyethylene + 7% of lithium

3.1 Simulations

The Ar activity at the end of a treatment is derived from the number of atoms of argon-41 created by irradiation, calculated by a reaction rate tally in the room air, as explained in paragraph 2.3. To calculate the multiplicative constant to be used, we need to determine the number of ^{40}Ar atoms present in the room air. Since the room interior has a volume of $(330 \cdot 400 \cdot 600) \text{ cm}^3 = 79.2 \cdot 10^6 \text{ cm}^3$, the number

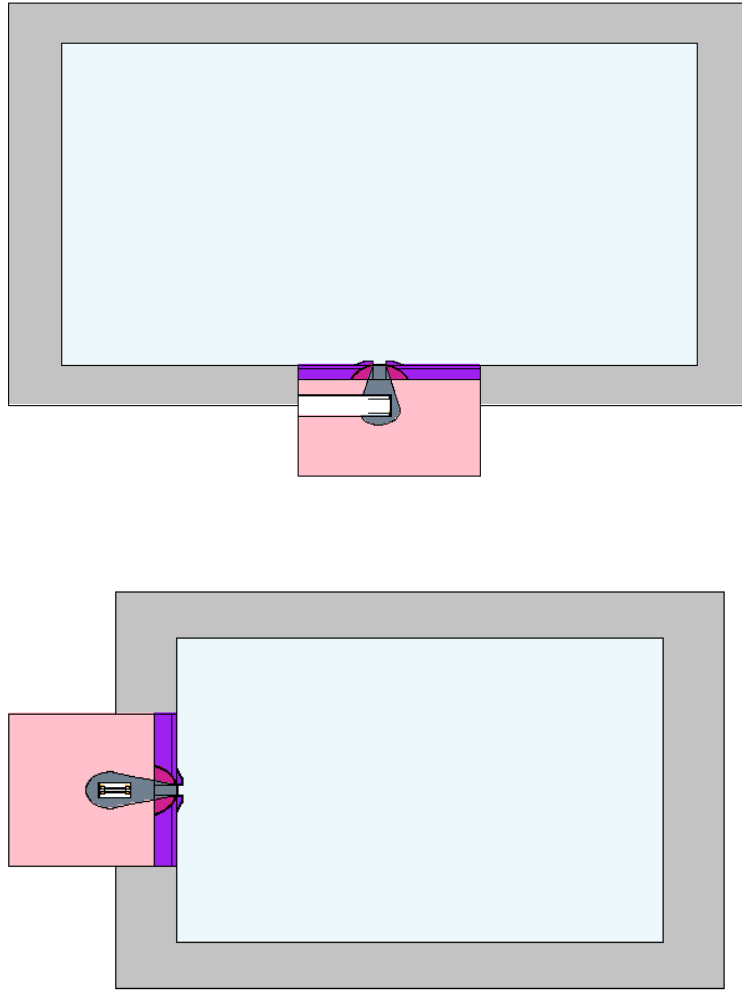


Figure 3.1: MCNP6 geometry of the treatment room (horizontal and vertical sections)

of ^{40}Ar atoms in the room (see Eq. 2.1) is equal to:

$$N = \frac{m_{\text{Ar-40}} \cdot N_A}{A_{\text{Ar-40}}} = \frac{\rho_{\text{air}} \cdot V_{\text{air}} \cdot \%_{\text{Ar/air}} \cdot \%_{\text{ISO}_{\text{Ar-40}}} \cdot N_A}{A_{\text{Ar-40}}} \quad (3.1)$$

where $\%_{\text{Ar/air}}$ is the percentage of argon in air, 0.934%, and $\%_{\text{ISO}_{\text{Ar-40}}}$ indicates the isotopic abundance of ^{40}Ar , 99.6%. Thus N is:

$$N = \frac{1200 \text{ g/m}^3 \cdot 79.2 \text{ m}^3 \cdot 0.934\% \cdot 99.6\% \cdot 6.022 \times 10^{23} \text{ mol}}{40 \text{ g/mol}} = 1.331 \times 10^{25} \quad (3.2)$$

The multiplicative constant C is then given by:

$$C = N \cdot 10^{-24} \cdot I = 127.776 \times 10^{13} \quad (3.3)$$

where I is the source intensity and 10^{-24} the conversion factor from barn to cm^2 . The reaction rate R gives the number of atoms of argon-41 created by irradiation

per unit time, providing the activity production rate in air due to this reaction. To obtain the final air activity, it is necessary to take into account the decay of ^{41}Ar . In addition, the ventilation system of the room decreases the air activity, by expelling part of activated argon. The rate of air replacements, that will be 15 per hour at CNAO, can be described as a decay constant (λ_{air}) that is added to the radioactive decay constant (λ_{phys}). Therefore the time evolution of air activity is overall given by:

$$\frac{dA}{dt} = A_{created} - A_{eliminated} = R\lambda_{phys} - (\lambda_{phys} + \lambda_{air})A \quad (3.4)$$

For Ar-41 λ_{phys} equals to $(157.7 \text{ minutes})^{-1}$, while λ_{air} is 15/hour i.e. 0.25/minute. At equilibrium $\frac{dA}{dt} = 0$, thus:

$$A = \frac{R \lambda_{phys}}{\lambda_{phys} + \lambda_{air}} \quad (3.5)$$

Since $\lambda_{phys} \ll \lambda_{air}$ we can neglect λ_{phys} at the denominator, thus the following relation holds for the final specific activity of air:

$$a = \frac{A}{m} = \frac{R \lambda_{phys}}{\lambda_{air} m} \quad (3.6)$$

The specific activity in air have been calculated in the described way for the walls composition listed above and compared with the limit of 1 Bq/g.

The simulations have been performed with open beam, but it must be considered that the real configuration in the treatment room will be with the patient in front of the beam. Therefore, the air activation has been evaluated also implementing a human phantom in the room geometry. The phantom used is MIRD (Fig. 3.2), a geometrical anthropomorphic model that resemble the human anatomy with 22 internal organs and more than 100 sub-regions [7]. MIRD was used to represent the patient also in the simulations described further in this thesis. Fig. 3.3 shows the room with MIRD phantom in a representative position for a clinical treatment.

3.2 Results

The reaction rates of $^{40}\text{Ar}(n,\gamma)^{41}\text{Ar}$ obtained by simulations with different walls compositions are listed in Table 3.1.

Walls composition	R [s^{-1}]
concrete	$(2.110 \pm 0.017) \times 10^7$
concrete + boron	$(2.624 \pm 0.005) \times 10^5$
polyethylene	$(9.660 \pm 0.015) \times 10^6$
polyethylene + lithium	$(8.339 \pm 0.018) \times 10^5$

Table 3.1: Simulated reaction rates for the activation of argon-40 with open beam

To verify the accuracy of the simulation, we have compared the simulated R with the one resulting from the simulated flux. The calculation of reaction rate is difficult

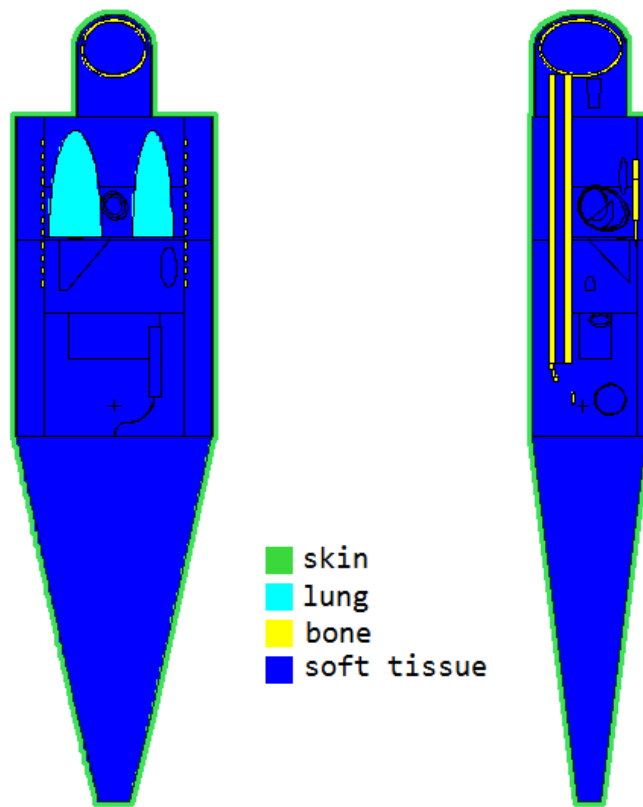


Figure 3.2: Coronal and sagittal sections of MIRD phantom

due to the integration over the energy range (as seen in Eq. 2.7), however, considering that activation is mainly produced by thermal neutrons, a good approximation is given by the relation $R = \phi N \sigma$, where ϕ is the flux in the thermal range, N the number of argon-40 nuclei in the room (see Eq.3.2) and σ the thermal capture cross section of $^{40}\text{Ar}(n,\gamma)^{41}\text{Ar}$, 0.7 barn [8]. The values of ϕ for the different walls compositions have been simulated with an F4:n tally (neutron fluence) in the thermal energy range in the whole room volume, and are listed in Table 3.2 along with the reaction rates obtained from them through $R = \phi N \sigma$. Results in Table 3.1 and 3.2 are in good agreement.

The specific activities in air obtained for each walls composition through Eq. 3.6 are listed in Table 3.3.

Boron-loaded concrete results to be the best choice for the walls composition: unlike the other materials, it allows the slowing down of neutrons and their capture from boron through the same reaction of BNCT. The particles created have a very small range in the walls so they do not contribute to room activity. Moreover, as opposed to polyethylene, concrete is capable of shielding the gammas, and with such addition of boron is a material technologically easily obtainable.

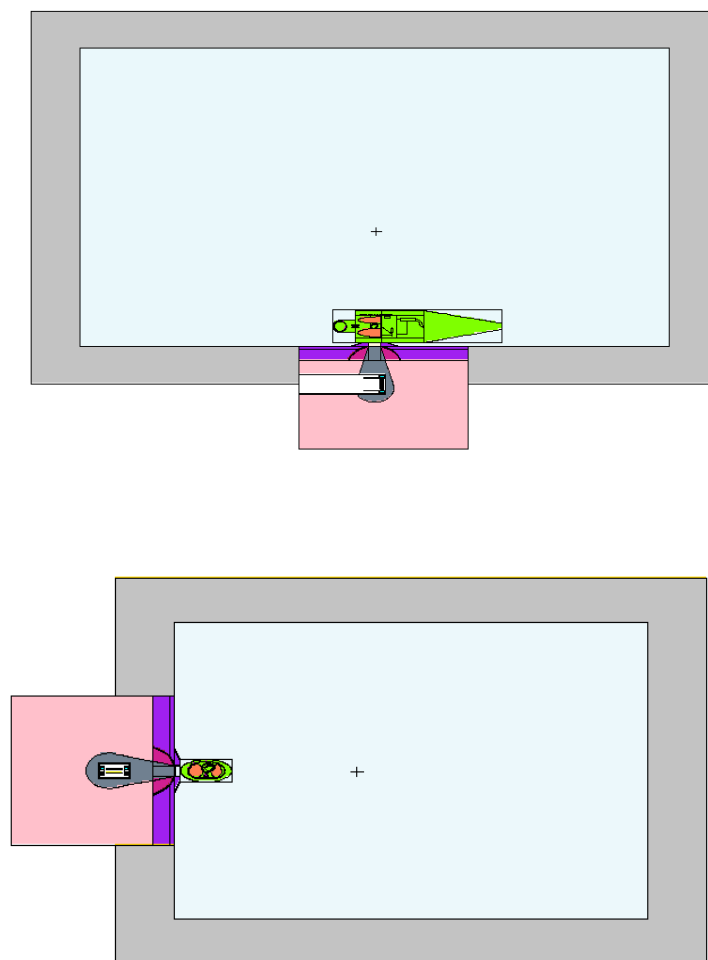


Figure 3.3: Representation of room geometry (horizontal and vertical sections) with MIRD phantom positioned for a clinical treatment

Assessed that borated concrete is the best material to use for the wall composition, we have implemented MIRD phantom in the room with walls made of ordinary and boron-loaded concrete, obtaining the values shown in Table 3.4.

With the walls made of boron-loaded concrete, ^{41}Ar production does not exceed the limit of 1 Bq/g, even in the most conservative situation where the beam is open without the patient. Interestingly, with walls of ordinary concrete, the presence of MIRD at the beam port produces higher air activation compared with the open beam alone.

The results obtained confirm the possibility of using the treatment room with the optimized beam, provided the presence of an acceptable percentage of ^{10}B in the walls concrete, ensuring compliance with the design goal regarding air activation.

Walls composition	ϕ [$\text{cm}^{-2} \text{s}^{-1}$]	$R = \phi N \sigma$ [s^{-1}]
concrete	$(2.794 \pm 0.002) \times 10^6$	$(2.604 \pm 0.002) \times 10^7$
concrete + boron	$(1.605 \pm 0.009) \times 10^4$	$(1.495 \pm 0.008) \times 10^5$
polyethylene	$(1.283 \pm 0.002) \times 10^6$	$(1.195 \pm 0.019) \times 10^7$
polyethylene + lithium	$(1.041 \pm 0.003) \times 10^5$	$(9.70 \pm 0.03) \times 10^5$

Table 3.2: Simulated thermal fluxes with open beam and reaction rates calculated

Walls composition	a [Bq/g]
concrete	5.632 ± 0.005
concrete + boron	0.07004 ± 0.00014
polyethylene	2.578 ± 0.004
polyethylene + lithium	0.2226 ± 0.0005

Table 3.3: Air specific activity in the room due to argon activation with open beam

Walls composition	R [s^{-1}]	a [Bq/g]
concrete	$(2.007 \pm 0.002) \times 10^7$	5.357 ± 0.006
concrete + boron	$(3.9450 \pm 0.0001) \times 10^5$	0.1053 ± 0.0003

Table 3.4: Reaction rate and air activity with MIRD phantom at the beam port

Chapter 4

Patient and air dosimetry

In the previous Chapter, concrete was demonstrate to be a better candidate than polyethylene as far as the activation is concerned. In this Chapter, simulations of dose distributions in the room and in patients are presented. The geometry is the same presented in the last Chapter, with the walls made of concrete and boron-loaded concrete.

4.1 Air dosimetry

To calculate dose distribution in air, simulations were run with and without the MIRD phantom, and a F4 MESH tally has been used to evaluate the dose distribution in the room air. In MCNP the use of MESH leads to a space reticulation independent from geometry and allows the visualization of results in a colour-scale plot. In our case we have chosen a MESH "lattice" with units of $10 \times 15 \times 20 \text{ cm}^3$, as shown in Fig. 4.1.

The dose from neutrons is determined from kerma assuming CPE conditions, i.e. Charged-Particle Equilibrium, the situation in which, for each energy and particle type, the number of charged particles leaving a volume is equal to the number of particles entering the same volume. When CPE occurs in an irradiated medium, kerma in the volume is equal to the absorbed dose [13]. We can reasonably assume that this situation is verified in the volumes studied in our simulations.

Thus, a tally of type F4 was required, coupled with the DE+DF factors for the fluence conversion. This syntax leads to the division of energy range of the problem according to the binning indicated by DE values, and to the multiplication of the neutron fluence in each energy bin by the kerma factor in DF corresponding value. This calculation gives the kerma (which, as mentioned above, is equal to absorbed dose in CPE) for neutrons in such energy range. Then MCNP6 provides, as result of the tally, the sum over all energy bins, i.e. the total absorbed dose in the volume.

We have used the neutron kerma factors for Medical Physics Air, calculated from kerma data in ICRU Report 63 and JENDL-3.2 cross sections and Q-values (kerma factors from [14]), thus obtaining the absorbed dose in air.

We have also added two FMESH:4 tallies with different DE+DF to simulate two typical quantities used in radiation protection: the equivalent dose, H, and the ambient dose equivalent $H^*(10)$, as explained in the following paragraphs.

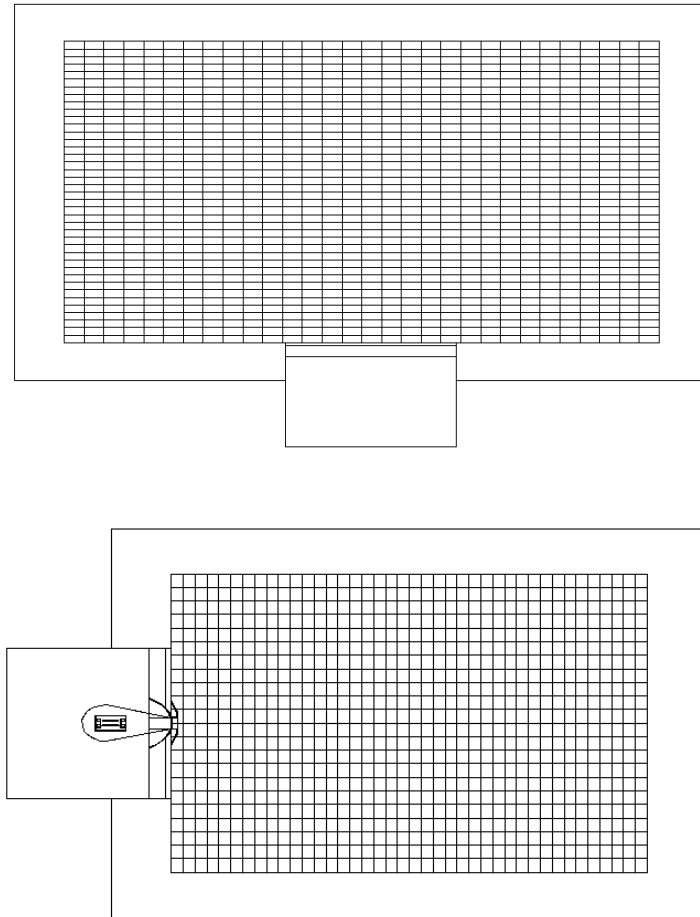


Figure 4.1: MCNP6 geometry of the room (horizontal and vertical sections) with MESH reticulation

4.1.1 Equivalent dose

Equivalent dose, H , is a protection quantity¹ used in radiological protection, that takes into account the biological effectiveness of the radiation. H is calculated from the mean absorbed dose deposited in a body tissue or organ T , multiplied by a radiation weighting factor w_R , depending on the type and energy of the radiation R :

$$H_T = \sum_R w_R \cdot D_{T,R} \quad (4.1)$$

The weighting factors represent the RBE (Relative Biological Effectiveness) of the radiation (they are related to LET, Linear Energy Transfer) and modify the absorbed dose according to the different biological effects of various types and energies of radiation. The International Committee for Radiation Protection (ICRP) has assigned radiation weighting factors for various radiation types. We have used the factors of

¹Not a physical quantity, since its definition can change over time, depending on the different decisions of the Commissions for Radiation Protection, which establish the values of the factors to be used.

ICRP Publication 116 for neutrons, given as a continuous function of neutron energy E_n as follows:

$$w_R = \begin{cases} 2.5 + 18.2 e^{-[\ln(E_n)]^2/6} & \text{for } E_n < 1 \text{ MeV,} \\ 5.0 + 17.0 e^{-[\ln(2E_n)]^2/6} & \text{for } 1 \text{ MeV} \leq E_n \leq 50 \text{ MeV,} \\ 2.5 + 3.25 e^{-[\ln(0.04E_n)]^2/6} & \text{for } E_n > 50 \text{ MeV.} \end{cases} \quad (4.2)$$

To obtain the equivalent dose, a FMESH:4 tally has been used with DF values obtained from air kerma factors multiplied by the appropriate w_R .

4.1.2 Ambient dose equivalent

Ambient dose equivalent is the main quantity used in radiological protection for external monitoring of environments. It characterizes the potential irradiation of individuals, in terms of a dose equivalent quantity that would exist in a phantom approximating the human body. The phantom chosen is the ICRU sphere, made of 30-cm-diameter tissue-equivalent plastics with a density of 1 g/cm^3 and a mass composition of 76.2% oxygen, 11.1% carbon, 10.1% hydrogen and 2.6% nitrogen. The ambient dose equivalent, $H^*(d)$, at a certain point in a radiation field is the dose equivalent that would be produced by the corresponding expanded and aligned field at a depth d in the ICRU sphere, on the radius opposing the direction of the aligned field. For strongly penetrating radiations a reference depth d of 10 mm is recommended. Expanded radiation field is a hypothetical field where fluence and its angular and energetic distributions have the same values in the volume of interest as in the actual field at the point of reference. An expanded and aligned radiation field requires additionally a unidirectional fluence [16]. (Fig. 4.2)

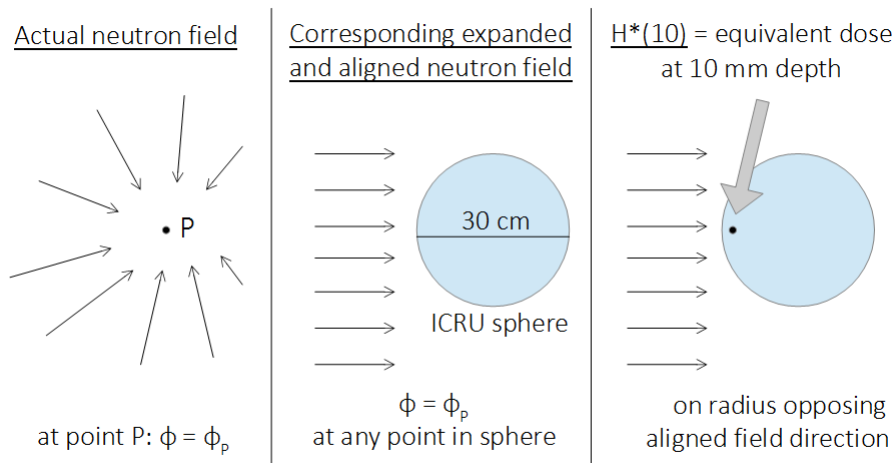


Figure 4.2: Expanded and aligned field and $H^*(10)$ representation

To obtain the ambient dose equivalent from MCNP6 we have used a FMESH:4 tally, with, as DE+DF, the factors needed for the conversion from fluence in $H^*(10)$ ([17],

[18]). MCNP6 is provided by a tally syntax that should produce $H^*(10)$ directly, however, due to a bug that has not been fixed in this version yet, it is incompatible with MESH use, thus the calculation was run with the conversion factors instead.

4.1.3 Results

Figures 4.3-4.5 show the dose distributions in air when walls are made of concrete, Figures 4.6-4.8 show the same distributions when walls are made of boron-loaded concrete. The doses have been evaluated for three neutron energy bins: thermal (0-0.4 eV), epithermal (0.4 eV-0.5 MeV) and fast (0.5-4 MeV). Figures 4.9 and 4.10 show the total distributions, i.e. the doses for the whole energy range from 0 to 4 MeV, for ordinary and borated concrete.

The distributions of doses with walls of borated concrete show a reduction with respect to the ones obtained with ordinary concrete, confirming the ability of loaded material in reducing the neutron flux in the room air.

The plots demonstrate also that the dose is higher along one side of the beam. We can attribute the cause of this asymmetry to the presence of vacuum channel in the accelerator structure, with respect to the full shielding material present on the opposite side. To eliminate this effect, a layer of lithium-loaded polyethylene, that absorbs excess neutrons, might be added in the wall in front of the vacuum tube.

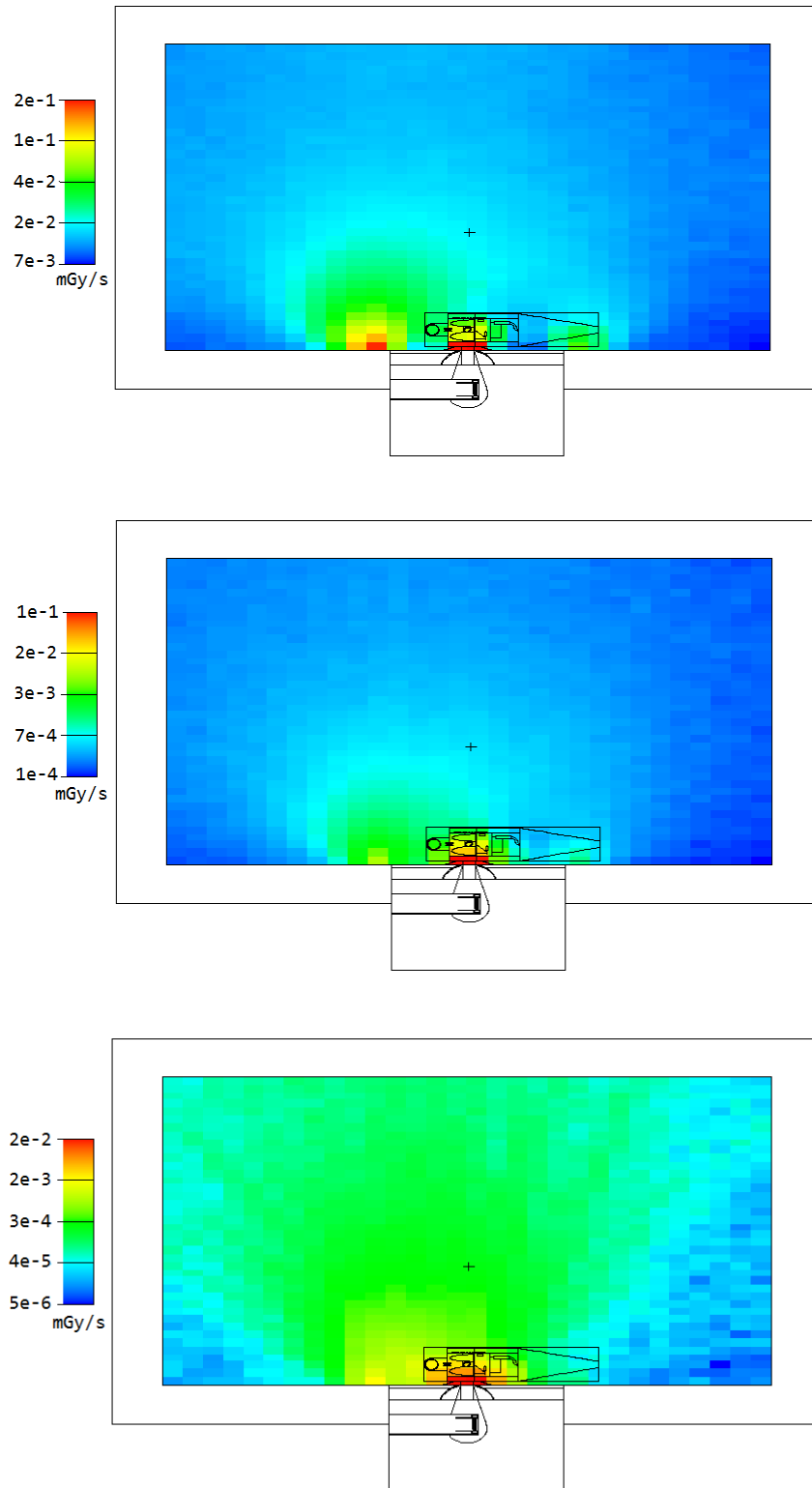


Figure 4.3: Absorbed dose MESH in the room air with walls of ordinary concrete (top: from thermal neutrons, center: from epithermal neutrons, bottom: from fast neutrons)

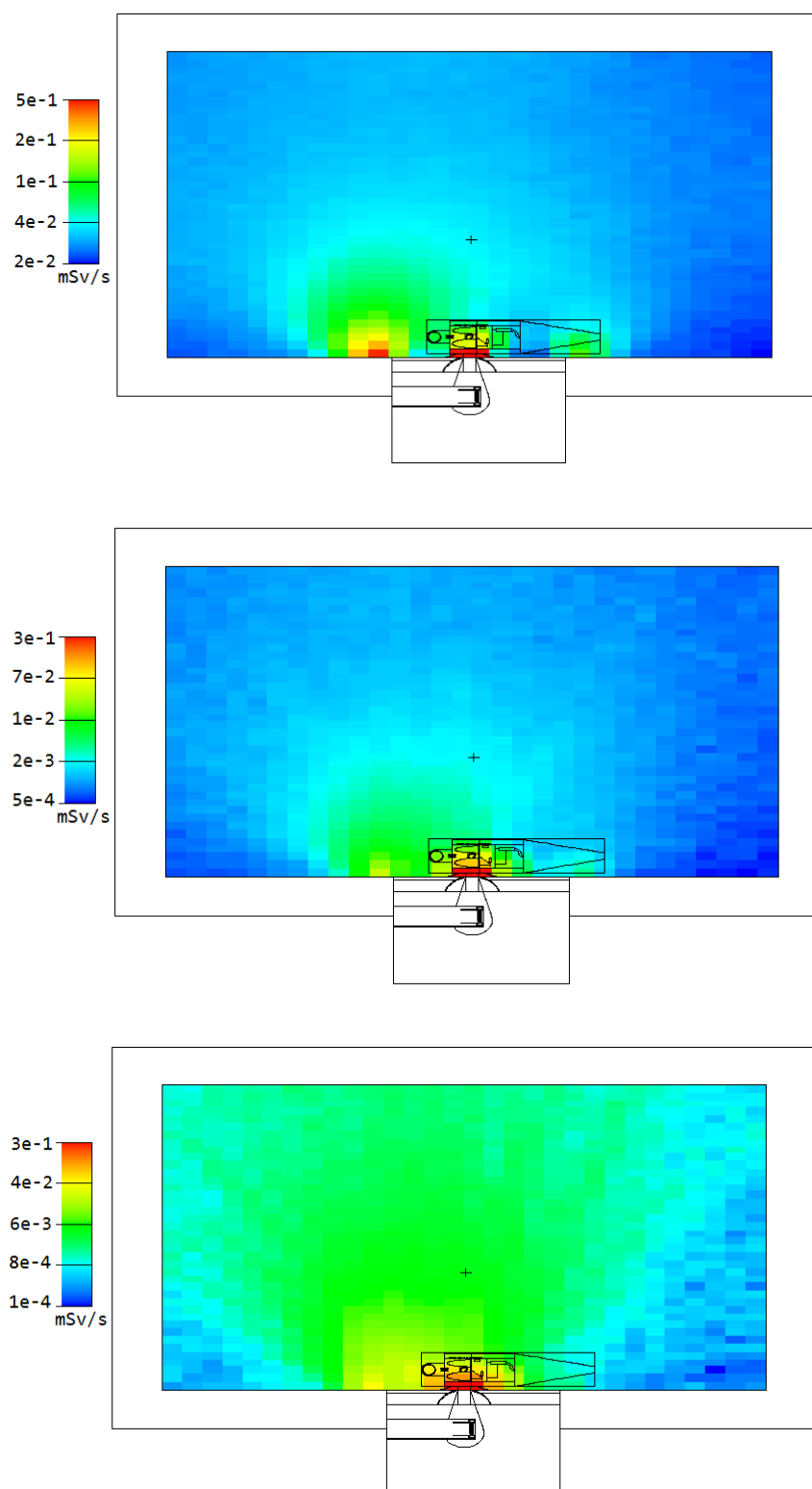


Figure 4.4: Equivalent dose MESH in the room air with walls of ordinary concrete (top: from thermal neutrons, center: from epithermal neutrons, bottom: from fast neutrons)

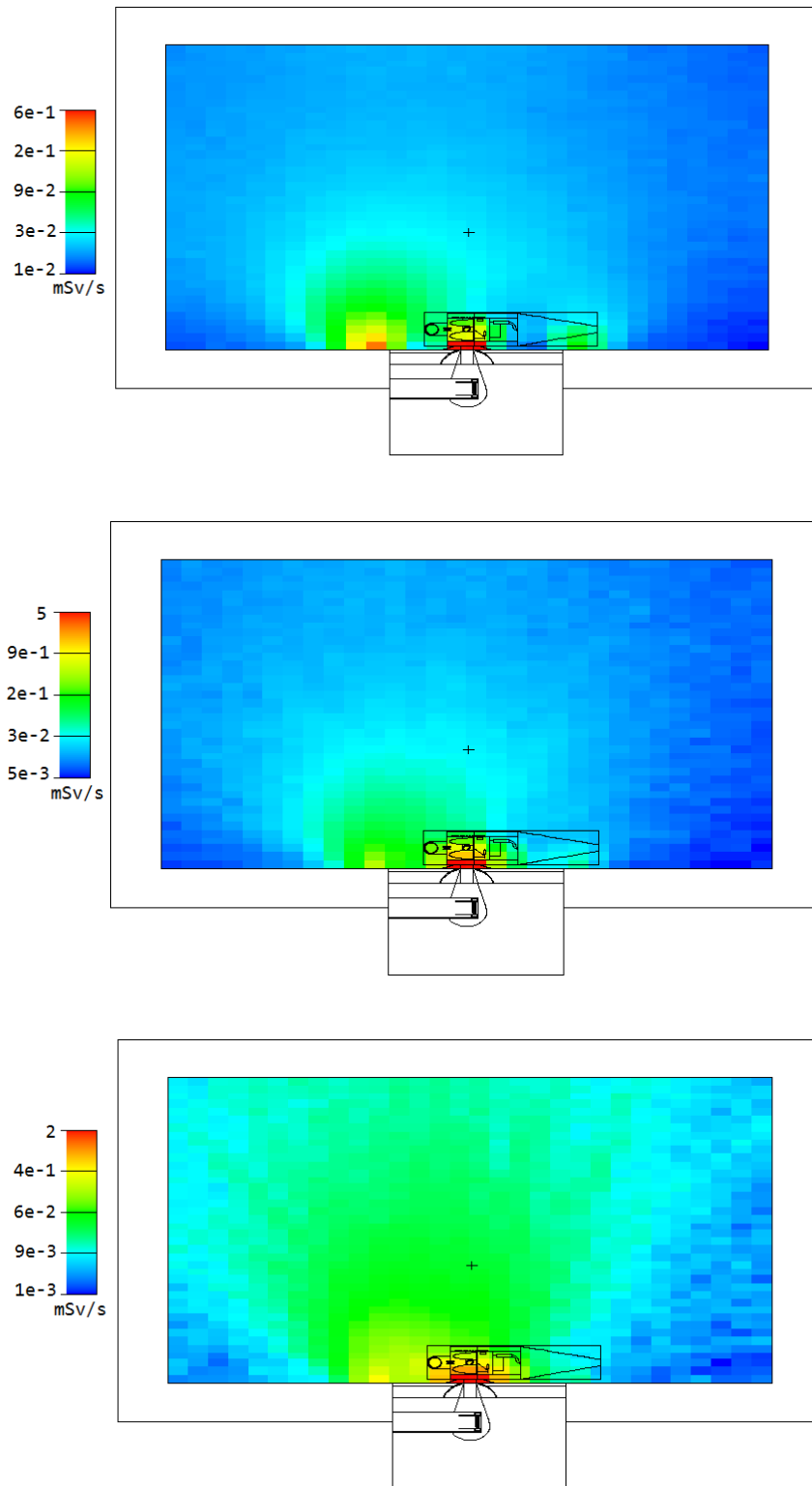


Figure 4.5: Ambient dose equivalent MESH in the room air with walls of ordinary concrete (top: from thermal neutrons, center: from epithermal neutrons, bottom: from fast neutrons)

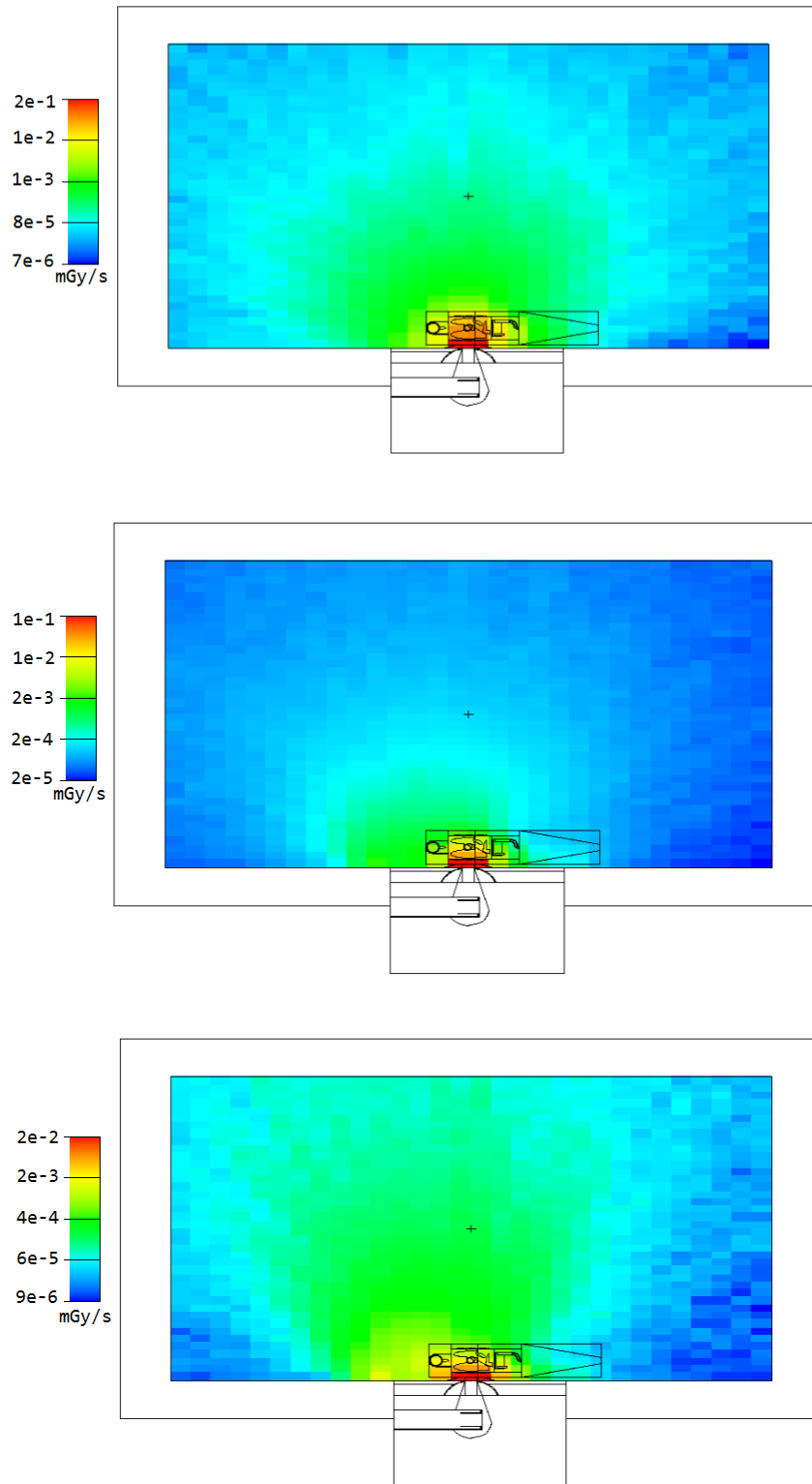


Figure 4.6: Absorbed dose MESH in the room air with walls of borated concrete (top: from thermal neutrons, center: from epithermal neutrons, bottom: from fast neutrons)

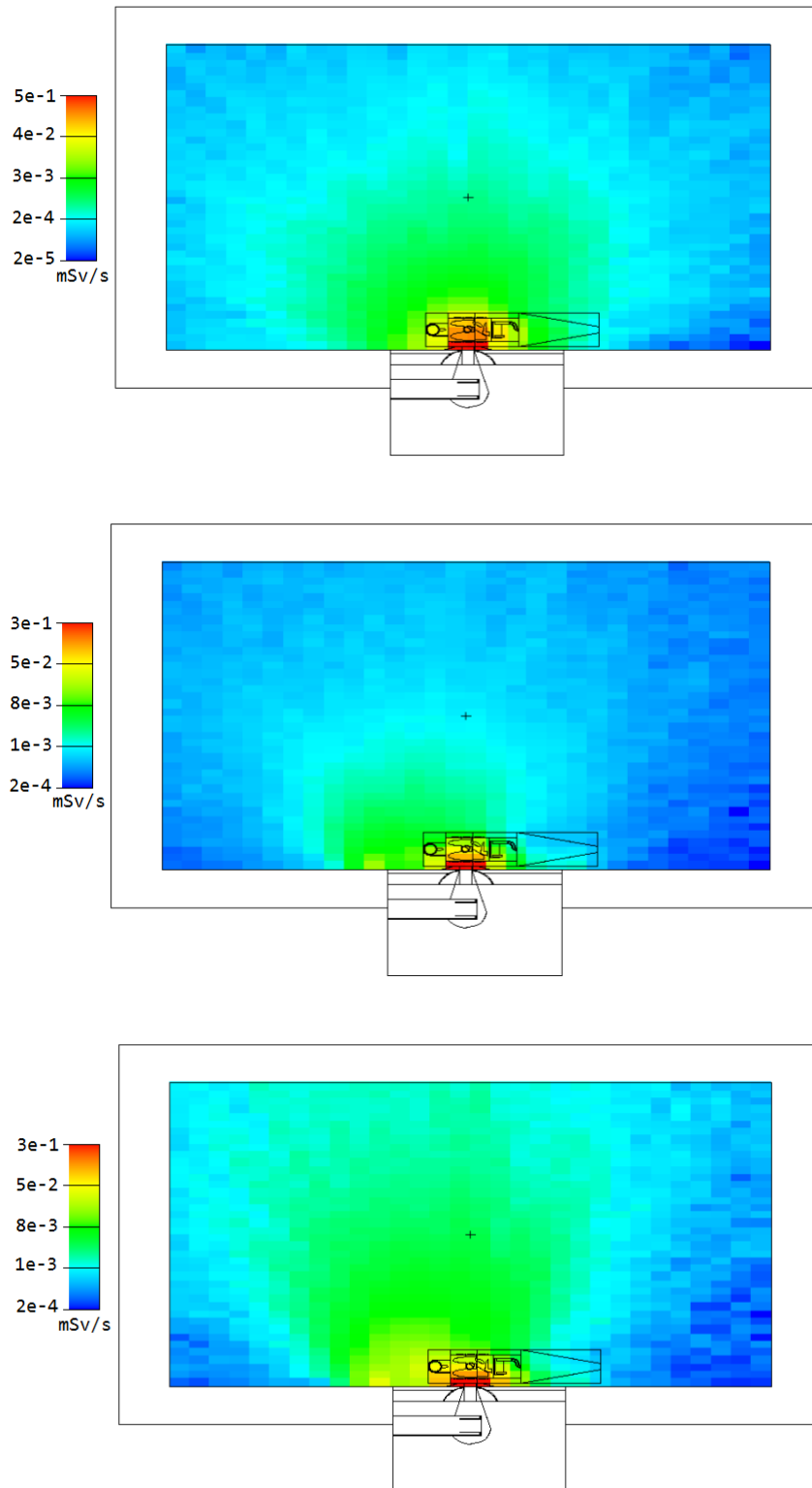


Figure 4.7: Equivalent dose MESH in the room air with walls of borated concrete (top: from thermal neutrons, center: from epithermal neutrons, bottom: from fast neutrons)

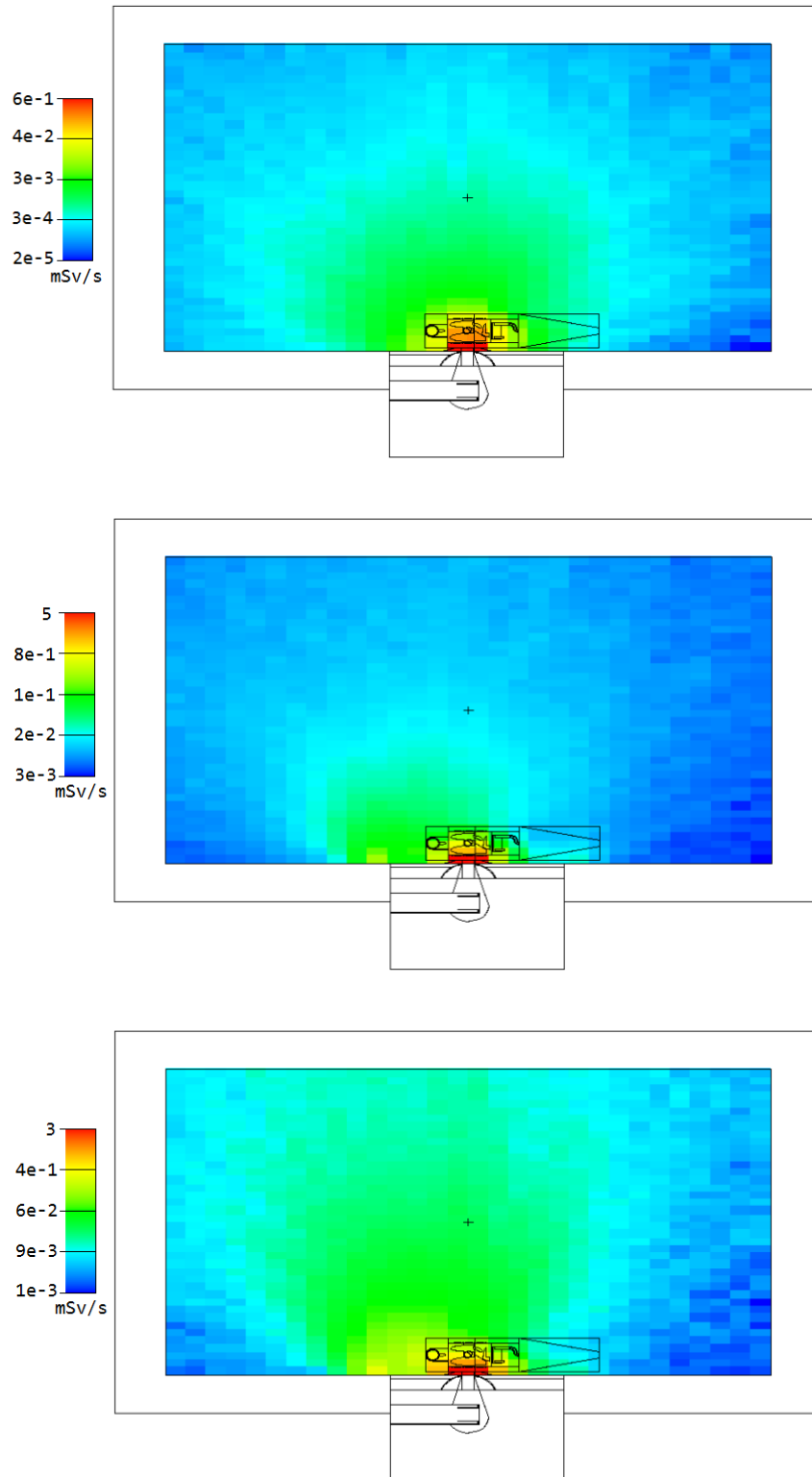


Figure 4.8: Ambient dose equivalent MESH in the room air with walls of borated concrete (top: from thermal neutrons, center: from epithermal neutrons, bottom: from fast neutrons)

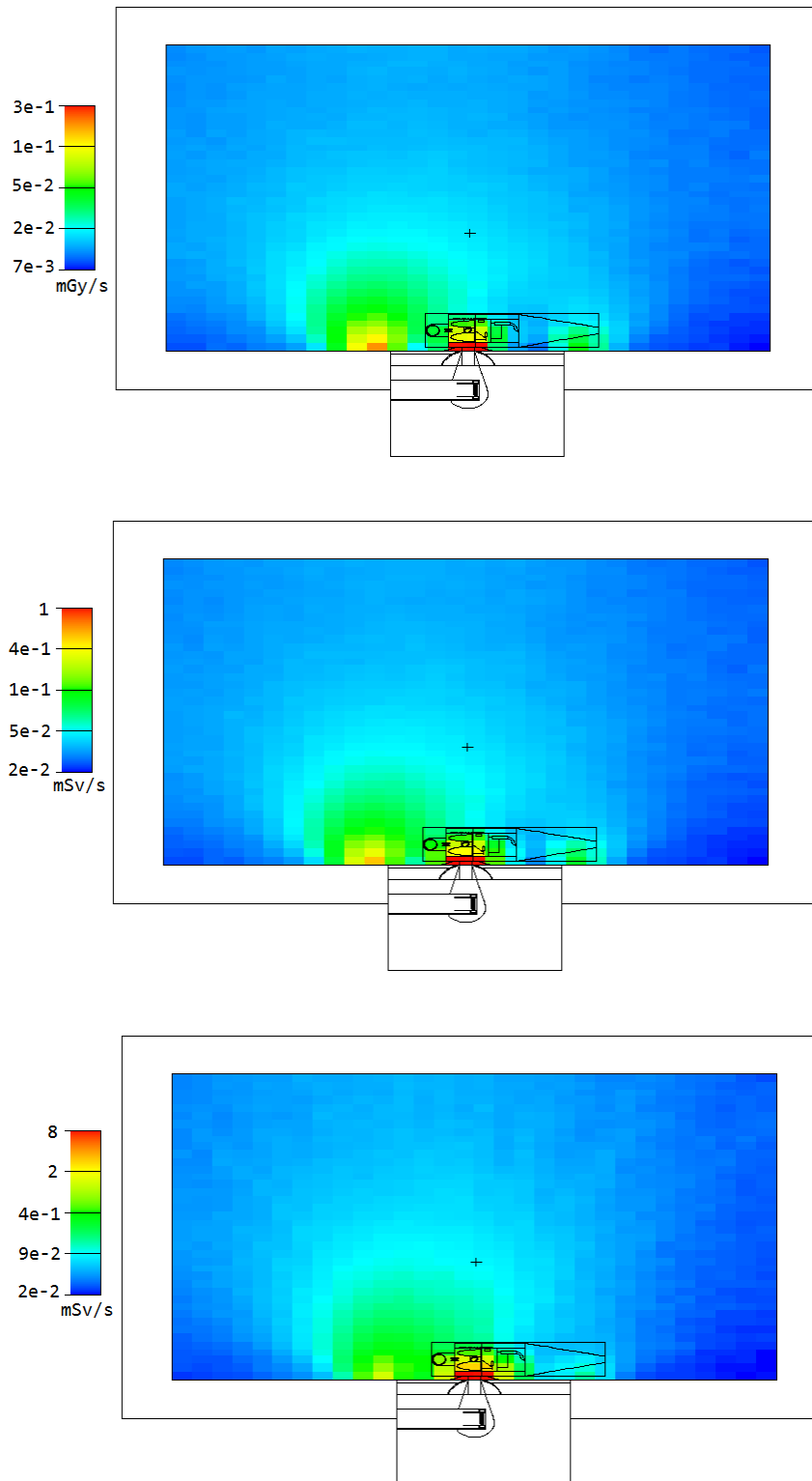


Figure 4.9: Total MESH of absorbed dose (top), equivalent dose (center) and ambient dose equivalent (bottom) in the room air with walls of ordinary concrete

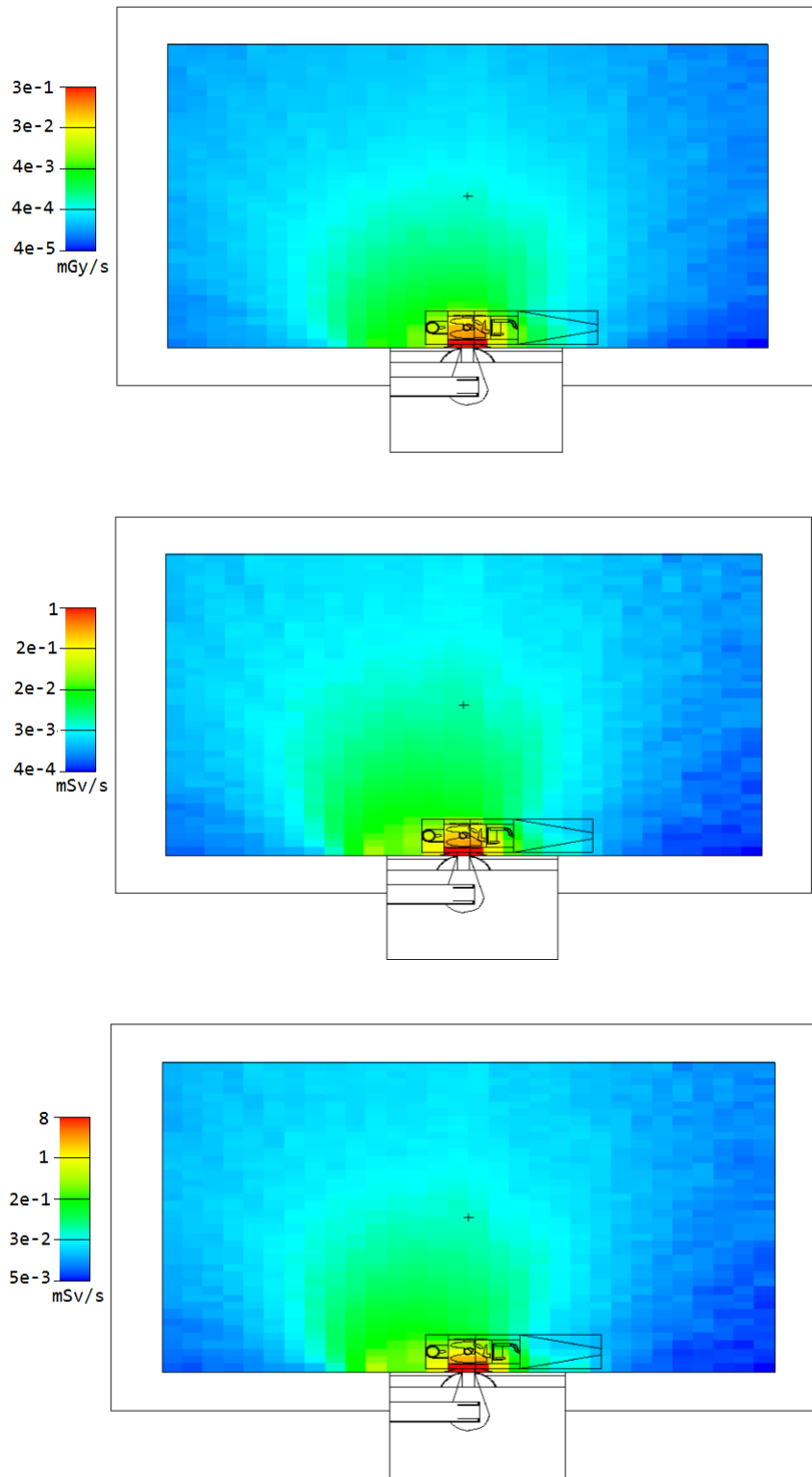


Figure 4.10: Total MESH of absorbed dose (top), equivalent dose (center) and ambient dose equivalent (bottom) in the room air with walls of borated concrete

4.2 Patient dosimetry

To study the dose in the patient, a clinical irradiation has been simulated with the MIRD phantom positioned in front of the beam, as shown in Fig. 3.3.

The doses received by the most relevant organs have been evaluated, considering the energy imparted from the nuclear reactions that occur in a biological tissue irradiated with neutrons. To take into account the boron enrichment needed for BNCT, we have conservatively considered 15 ppm of B in addition to the standard composition of human soft tissue². Overall the reactions involved are the following:

- radiative capture on hydrogen: ${}^1\text{H}(n,\gamma){}^2\text{H}$
- elastic scattering on hydrogen: ${}^1\text{H}(n,n){}^1\text{H}$
- capture with proton emission on nitrogen: ${}^{14}\text{N}(n,p){}^{14}\text{C}$
- capture with alpha emission on boron: ${}^{10}\text{B}(n,\alpha){}^7\text{Li}$

To evaluate the doses due to the last three we have used reaction rate tallies, since the release of energy comes from charged particles with a very short range in the tissue, not able to exit the cell of the tally. Therefore the dose can be calculated by multiplying the reaction rate per mass unit by the Q-value of the reaction, which accounts for the energy released to the medium. To make the tally return the dose in Gy, with Q-value in MeV in the multiplicative constant C we have also to include the conversion from MeV to Joules, in addition to that needed for the conversion from grams to kilograms. Definitely, C is calculated as:

$$C = I \cdot \frac{\% \cdot N_A}{A} \cdot (Q - \text{value}) \cdot 10^{-24} \cdot (\text{MeV} \rightarrow \text{J}) \cdot (g \rightarrow \text{kg}) \quad (4.3)$$

This applies to capture reactions: (n, p), reaction 103, and (n, alpha), reaction 107. In the case of elastic scattering on hydrogen, instead, MCNP allows to calculate the average energy released for each event of scattering. In this case the constant C only includes the source intensity, the number of atoms of H per gram and the conversions barn \rightarrow cm², MeV \rightarrow J and g \rightarrow Kg.

The dose due to the gamma rays produced by the radiative captures needs, instead, to be evaluated in a different way, since gammas have a mean free path large enough to leave the volume considered. Therefore in this case a F6:p tally is used: MCNP6 transports the photons created and calculates the energy released from them in the volume of interest. The result includes the energy related to secondary particles produced by gammas, considered all released at the point of their creation. In this way an approximation is made with regard to the electrons created, which actually would leave the volume if produced near the edges. This leads to a slightly overestimated dose, that however is a conservative approach in this case.

Since the tally result is energy imparted per unit mass, in MeV/g, to obtain the dose in Gray the conversions to Joules and to kilograms are needed. So the tally is modified by a multiplication factor M equal to

$$M = I \cdot (\text{MeV} \rightarrow \text{J}) \cdot (g \rightarrow \text{kg}) \quad (4.4)$$

²Since boron does not affect the neutron transport, MIRD composition was not modified. The 15 ppm concentration has been used to calculate the number of B atoms present in the tissue, for the dose evaluations via F4 tally.

4.2.1 Results

	Dose-rate [$\mu\text{Gy/s}$]				total
	(n,p)	(n, α)	(n,n)	(n, γ)	
brain	1.32 \pm 0.02	7.51 \pm 0.03	26.1 \pm 0.8	178.4 \pm 1.3	215 \pm 2
bladder	0.93 \pm 0.04	5.36 \pm 0.04	6.9 \pm 0.8	101 \pm 2	115 \pm 3
stomach	2.34 \pm 0.04	13.48 \pm 0.05	13.7 \pm 0.7	84.1 \pm 1.1	116.3 \pm 1.9
kidneys	2.36 \pm 0.05	13.6 \pm 0.05	17.5 \pm 0.9	109.8 \pm 1.5	146 \pm 2
intestine	2.05 \pm 0.03	11.78 \pm 0.04	19.0 \pm 0.7	138.1 \pm 1.1	173.3 \pm 1.9
lungs	5.49 \pm 0.03	31.50 \pm 0.04	89.8 \pm 0.9	6.05 \pm 0.03	139.2 \pm 1.0
liver	6.41 \pm 0.06	36.82 \pm 0.06	65.9 \pm 1.2	221.1 \pm 1.5	338 \pm 3

Table 4.1: Dose-rate in the principal organs with walls of ordinary concrete

The organs considered are brain, bladder, stomach, kidneys, intestine, lungs and liver. Dose-rates have been evaluated with the walls made of ordinary and boron-loaded concrete, and are listed in Table 4.1 and 4.2, showing a general decrease in the case of the loaded material. For each organ considered the main contribution comes from the radiative capture on hydrogen, except for lungs, which present a very low stopping power for gammas due to their composition (air, substantially). In the case of lungs the higher value is due to elastic scattering on hydrogen, the second principal contribution for the other organs. We can also note that the reaction (n, α) due to boron enrichment of tissues does not particularly affect the total dose-rate.

From the dose-rates obtained we have also evaluated the total dose absorbed in a treatment, assuming an irradiation lasting conservatively 2 hours. Results are shown in Table 4.3.

	Dose-rate [$\mu\text{Gy/s}$]				total
	(n,p)	(n, α)	(n,n)	(n, γ)	
brain	0.419 \pm 0.010	2.378 \pm 0.012	26.0 \pm 0.6	129.8 \pm 0.8	159.1 \pm 1.5
bladder	0.50 \pm 0.02	2.90 \pm 0.03	5.2 \pm 0.5	82.2 \pm 1.4	91.4 \pm 1.9
stomach	2.05 \pm 0.03	11.78 \pm 0.03	12.1 \pm 0.5	72.5 \pm 0.8	100.8 \pm 1.4
kidneys	2.04 \pm 0.03	11.72 \pm 0.04	16.2 \pm 0.7	92.6 \pm 1.0	124.9 \pm 1.8
intestine	1.62 \pm 0.02	9.32 \pm 0.03	19.3 \pm 0.5	120.1 \pm 0.8	152.2 \pm 1.4
lungs	4.99 \pm 0.02	28.65 \pm 0.03	91.4 \pm 0.7	5.35 \pm 0.02	136.1 \pm 0.8
liver	6.02 \pm 0.04	34.60 \pm 0.05	67.4 \pm 1.0	203.2 \pm 1.2	318 \pm 2

Table 4.2: Dose-rate in the principal organs with walls of boron-loaded concrete

	Dose in 2h [mGy]	
	ordinary concrete	concrete+boron
brain	773 \pm 7	573 \pm 5
bladder	415 \pm 11	329 \pm 7
stomach	419 \pm 7	363 \pm 5
kidneys	526 \pm 7	450 \pm 6
intestine	624 \pm 7	548 \pm 5
lungs	501 \pm 4	490 \pm 3
liver	122 \pm 11	115 \pm 7

Table 4.3: Doses absorbed by the principal organs in 2h of irradiation

Chapter 5

Activation of walls and patient

The last part of this work is devoted to evaluating the residual activity of the walls and of the patient. The residual activity has been determined starting from activation reaction rates, running simulations of a clinical irradiation with reaction rate tallies.

5.1 Walls activation

The composition used in the described simulations for ordinary concrete is the following¹:

	O	C	Ca	Al	K	Na	Fe	H	Mg	S
%	49.56	31.35	8.26	4.56	1.92	1.71	1.22	0.56	0.24	0.11

Hence, the reactions to be taken into account are:

- $^{27}\text{Al}(n,\gamma)^{28}\text{Al}$
- $^{40}\text{Ca}(n,\gamma)^{41}\text{Ca}$
- $^{58}\text{Fe}(n,\gamma)^{59}\text{Fe}$
- $^{41}\text{K}(n,\gamma)^{42}\text{K}$
- $^{26}\text{Mg}(n,\gamma)^{27}\text{Mg}$
- $^{23}\text{Na}(n,\gamma)^{24}\text{Na}$

For each of the reactions listed, we have simulated the reaction rate in the walls width to visualize the decreasing of residual radioactivity with the depth into the shielding. The normalization constant C for the tally has been calculated using the number of atoms of the target isotope, N , per volume unit:

$$C = \frac{N}{V} \cdot 10^{-24} \cdot I \quad (5.1)$$

¹Boron-loaded concrete has the same composition, added with 1% of B-10 and 4% of B-11, and the percentages of other elements re-scaled to a total of 95%.

In this way, the tally provides the number of activations per second per cm^3 . To better visualize the activation distribution in walls depth, a MESH has been used, as shown in Fig. 5.1.

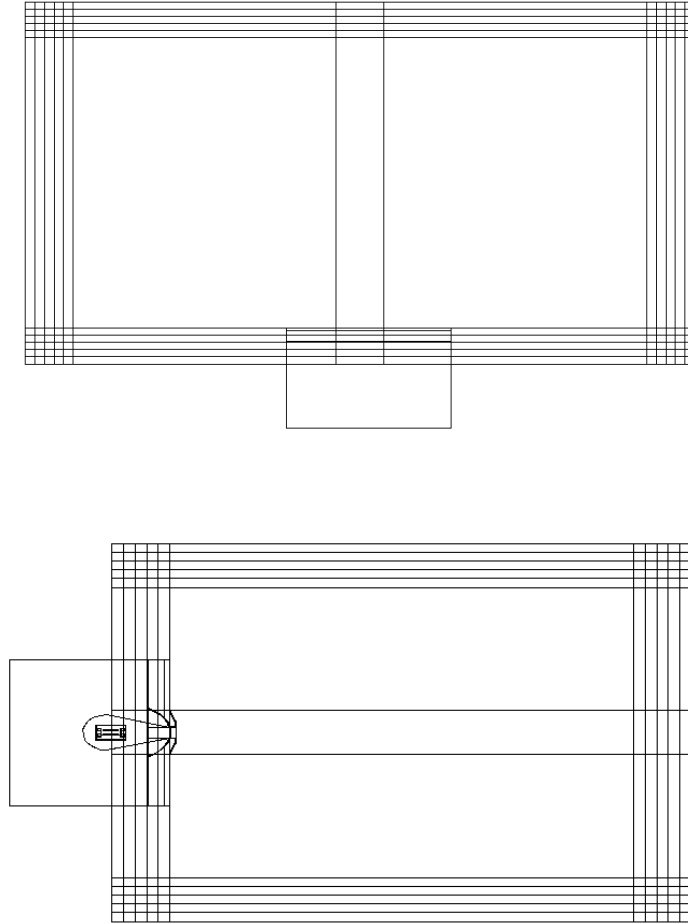


Figure 5.1: MCNP6 geometry of the room (horizontal and vertical section) with MESH reticulation of the walls depth

5.1.1 Results

Figures 5.2-5.5 show the activation reaction rates per cm^3 in the walls depth, for ordinary and boron-loaded concrete². Even in this case the borated concrete shows the best characteristics: on the first layer (in green in the figures) a reduction of a factor of about 100 is observed.

The neutron flux in the walls depth has also been evaluated with these simulations. The thermal, epithermal and fast flux meshes are represented in Fig. 5.6 for walls made of ordinary concrete, and in Fig. 5.7 for walls of boron-loaded concrete. In Fig. 5.8 the total fluxes for both walls composition are shown.

²The color discontinuity between the MESH bins in the wall of beam port is due to the great variability of simulated values in that region.

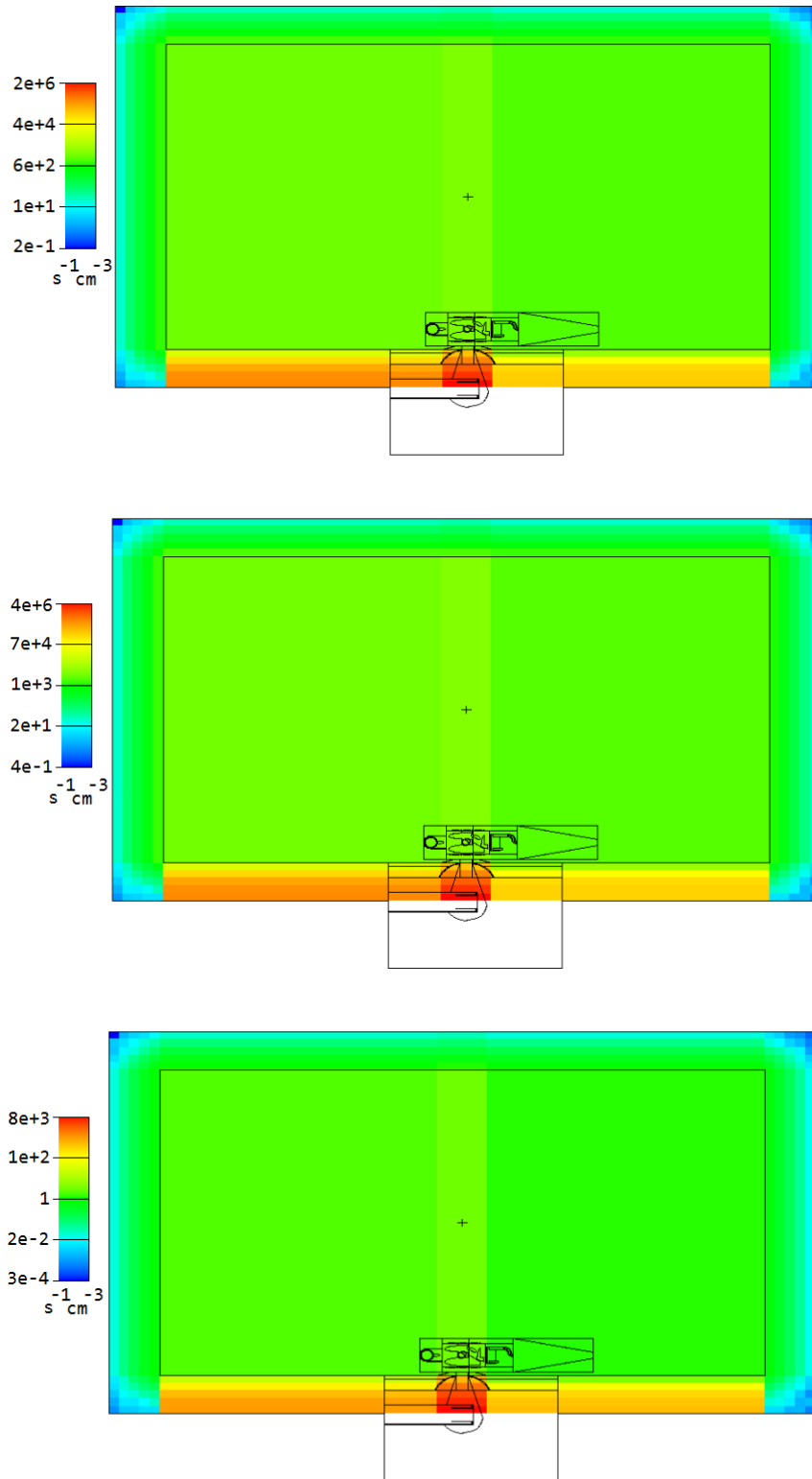


Figure 5.2: Activation MESH of ordinary concrete constituents (top: Al, center: Ca, bottom: Fe) in the walls

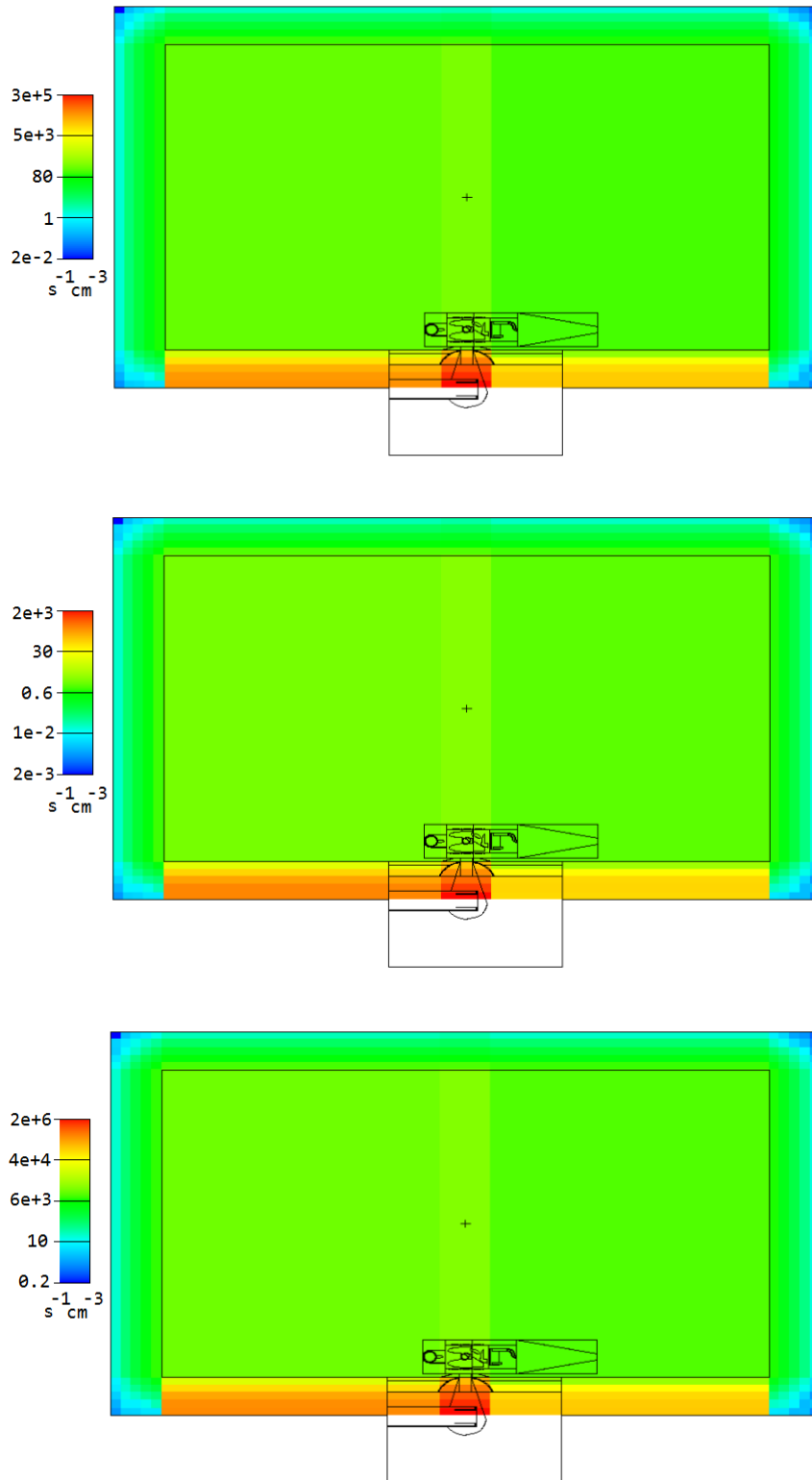


Figure 5.3: Activation MESH of ordinary concrete constituents (top: K, center: Mg, bottom: Na) in the walls

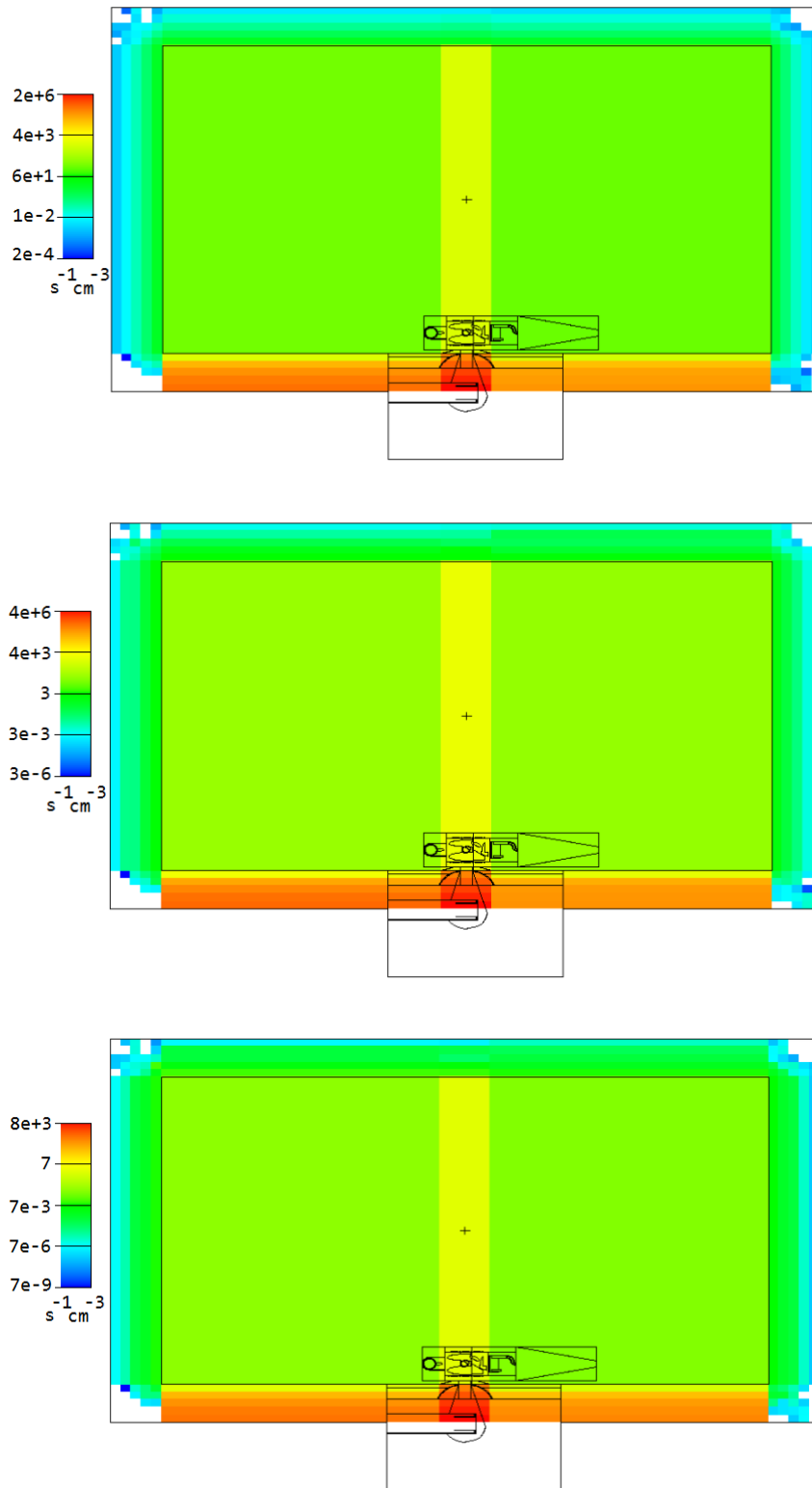


Figure 5.4: Activation MESH of boron-loaded concrete constituents (top: Al, center: Ca, bottom: Fe) in the walls

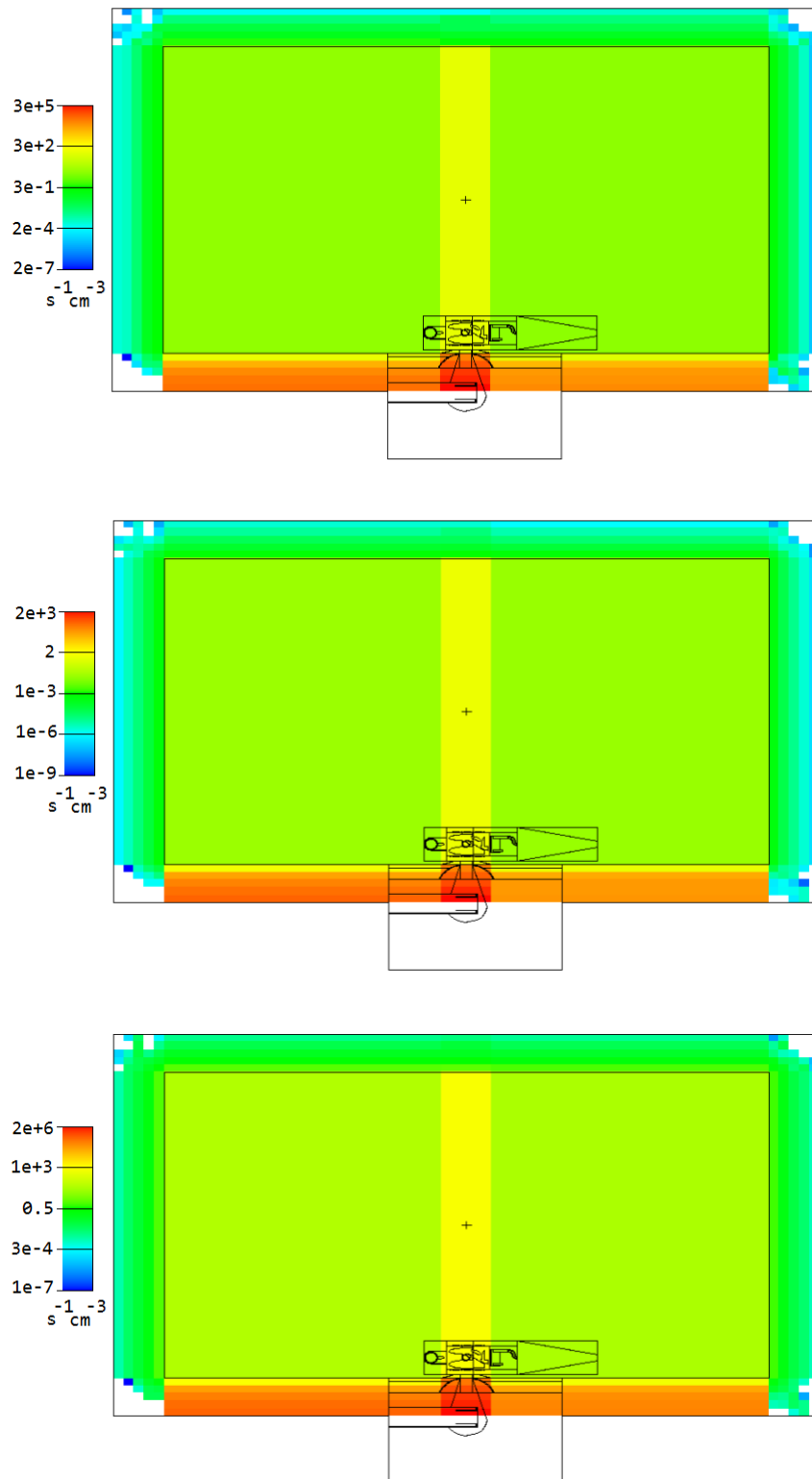


Figure 5.5: Activation MESH of boron-loaded concrete constituents (top: K, center: Mg, bottom: Na) in the walls

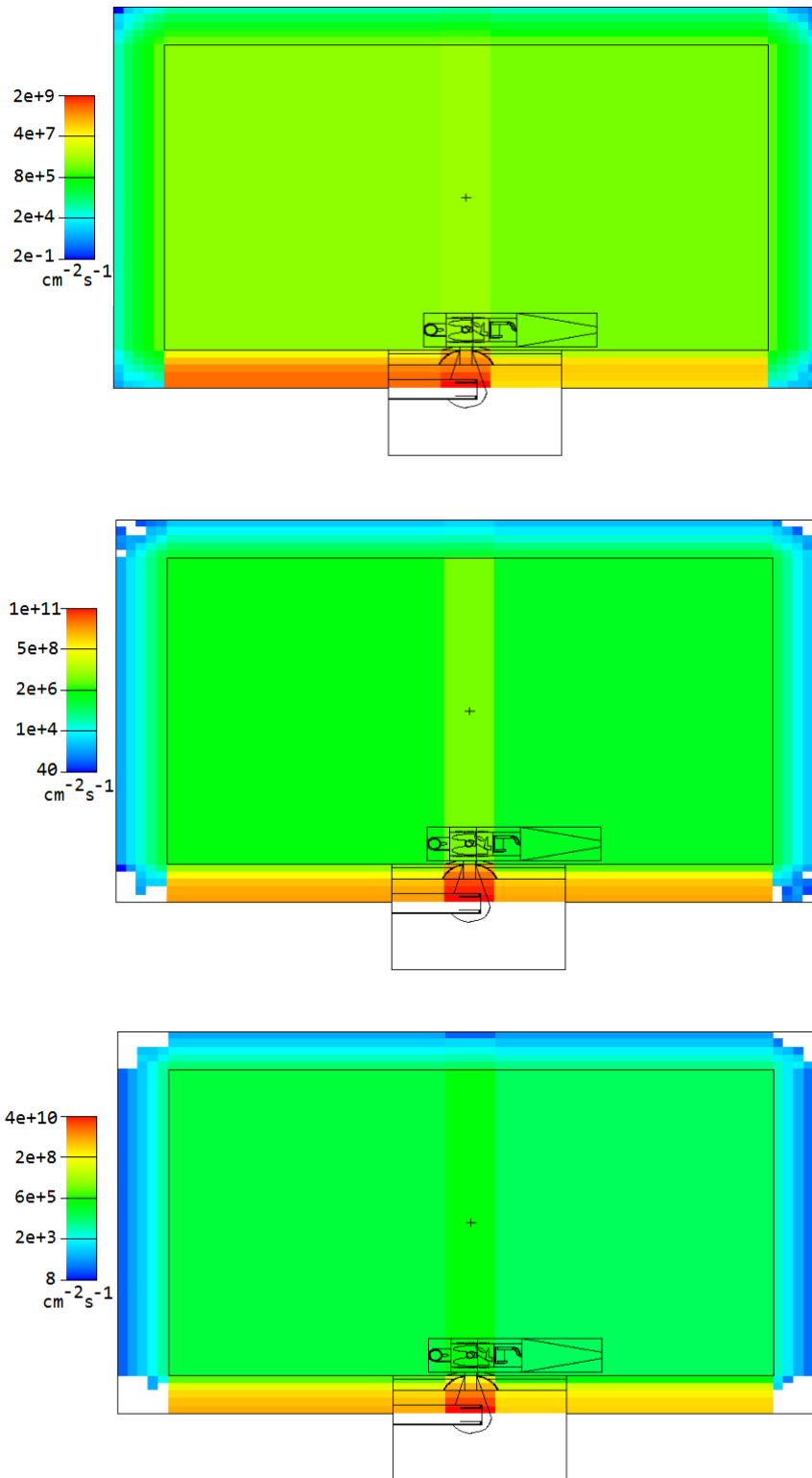


Figure 5.6: Neutron fluxes in the walls made of ordinary concrete (top: thermal flux, center: epithermal, bottom: fast)

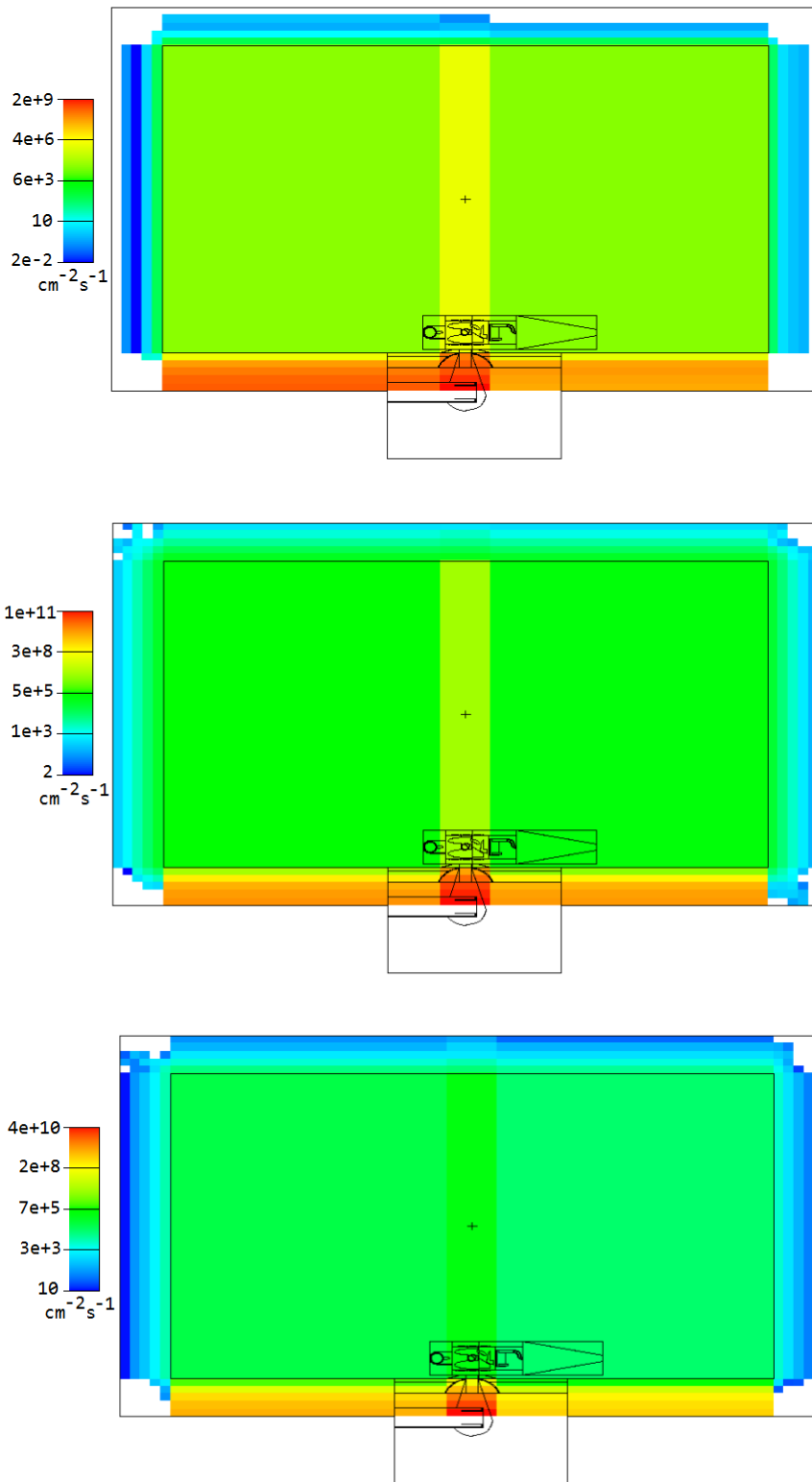


Figure 5.7: Neutron fluxes in the walls made of boron-loaded concrete (top: thermal flux, center: epithermal, bottom: fast)

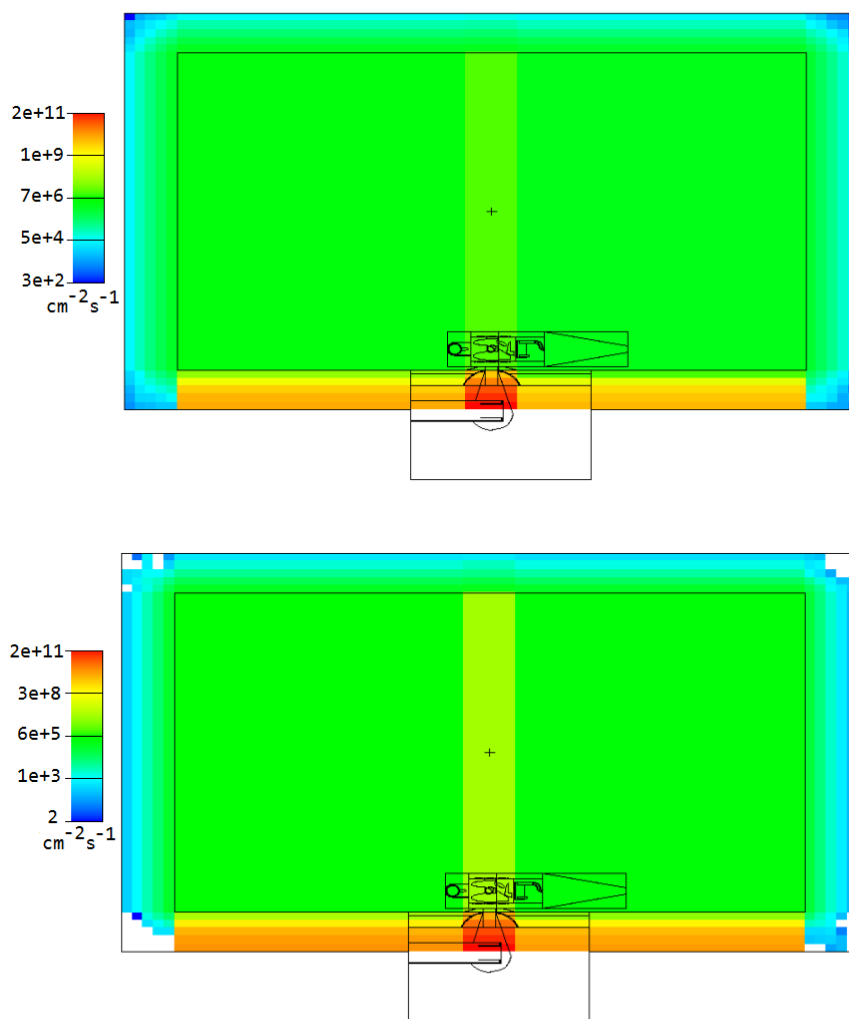


Figure 5.8: Total fluxes in the walls for ordinary (top) and borated (bottom) concrete

5.2 Patient activation

The residual activation of the patient body is an important aspect to be evaluated, also for the safety of those who will come into contact with the treated patients.

5.2.1 Urine activation

Urine contains some elements that activate due to neutron irradiation. Depending on the entity of the related residual activity, it may be necessary to consider the urine of treated patients as radioactive waste, thus to design specific facilities in the project of the building. To study this issue, we have simulated the activation of urine in a treatment, with MIRD phantom in the position described previously. The bladder content has been set with the following composition, from [19]:

	O	H	N	Cl	C	Na	K	P
%	86.2	11.0	1.0	0.6	0.5	0.4	0.2	0.1

Given the possible energies of neutrons reaching the bladder, not high enough for threshold reactions, the only reactions to be taken into account are:

- $^{37}\text{Cl}(n,\gamma)^{38}\text{Cl}$
- $^{41}\text{K}(n,\gamma)^{42}\text{K}$
- $^{23}\text{Na}(n,\gamma)^{24}\text{Na}$

The reaction $^{35}\text{Cl}(n,\gamma)^{36}\text{Cl}$ has not been considered, since chlorine 36 has a very long half-life of about $3 \cdot 10^5$ years, and it would not contribute much to the residual activity.

For the three reactions listed we have calculated the multiplicative constants to use for the reaction rate tallies. Being interested in activity per unit mass, C have been calculated through:

$$C = \frac{m\% \cdot N_A}{A} \cdot 10^{-24} \cdot I \quad (5.2)$$

From simulated reaction rates R , the residual activity after a conservative irradiation time of 2 hours has been evaluated, using Eq. 2.10.

Results

Reaction rates and residual activities were determined assuming walls of ordinary and boron-loaded concrete, and are listed respectively in Table 5.1 and 5.2. The decrease of the values in the second table compared to the first proves again the efficiency of boron-loaded concrete in reducing the thermal flux in the room. Residual activities obtained show that chlorine can be identified as the most problematic isotope. From these results it seems appropriate to think of a decay tank system to store the urine of treated patients.

Nuclide	Half-life [s]	R [$s^{-1} g^{-1}$]	a [Bq/g]
Cl-38	37.24 min	39.4 ± 1.9	26.5 ± 1.3
K-42	12.360 h	11.0 ± 0.5	0.60 ± 0.03
Na-24	14.9590 h	211 ± 10	9.6 ± 0.5

Table 5.1: Simulated reaction rates and specific activities after 2h of irradiation for urine elements, with walls of ordinary concrete

Nuclide	Half-life [s]	R [$s^{-1} g^{-1}$]	a [Bq/g]
Cl-38	37.24 min	23.9 ± 1.2	16.1 ± 0.8
K-42	12.360 h	6.7 ± 0.3	0.36 ± 0.02
Na-24	14.9590 h	128 ± 6	5.8 ± 0.3

Table 5.2: Simulated reaction rates and specific activities after 2h of irradiation for urine elements, with walls of boron-loaded concrete

5.2.2 Body activation

For the activation of the entire body of the patient, the MIRD was impossible to use due to its very complex geometry made of many separated cells, making the calculation of a tally in the whole volume too difficult. We have then substituted it with a much more simplified phantom: a rectangular parallelepiped with dimension $40 \times 15 \times 170 \text{ cm}^3$, and with composition equal to the soft tissue of MIRD. In Fig. 5.9 the phantom positioned in the room geometry is shown. Obviously the total volume of the phantom is overestimating the real one of a person, but for our purposes it is appropriate to be conservative.

The soft tissue used is so constituted:

	O	C	H	N	P	S	Cl	K	Fe
%	43.9	41.4	10.5	3.4	0.1	0.02	0.02	0.02	0.01

The activation reactions to be considered are:

- $^{37}\text{Cl}(n,\gamma)^{38}\text{Cl}$
- $^{58}\text{Fe}(n,\gamma)^{59}\text{Fe}$
- $^{41}\text{K}(n,\gamma)^{42}\text{K}$

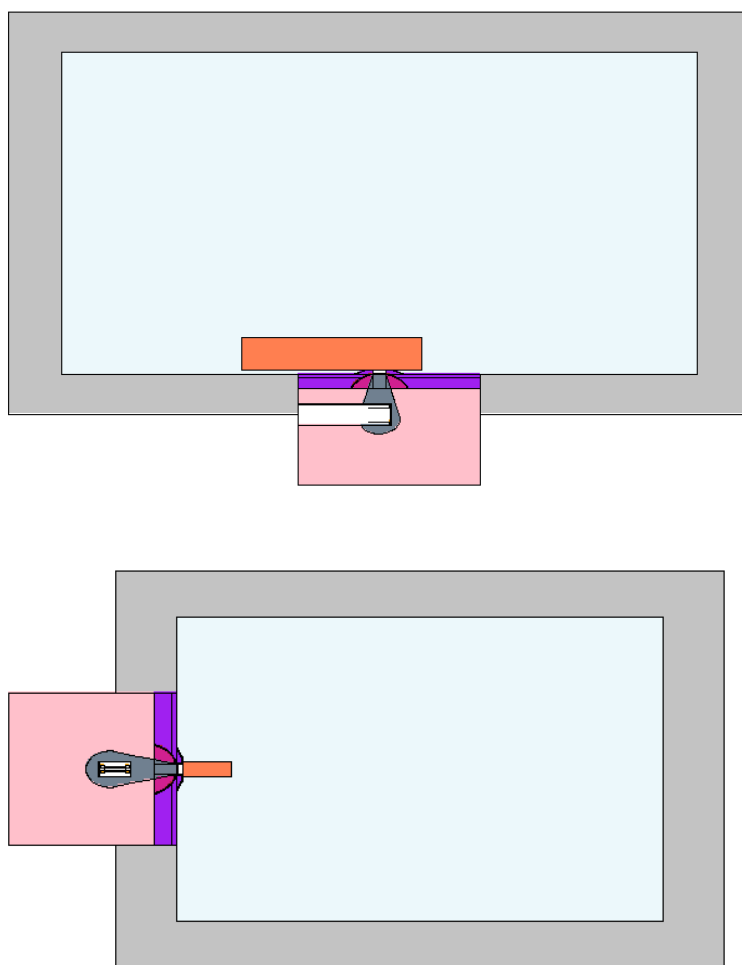


Figure 5.9: MCNP6 geometry of the room with parallelepiped phantom (horizontal and vertical sections)

Results

The reaction rates and specific activities after 2 hours of irradiation are listed in Table 5.3 (assuming walls of ordinary concrete) and Table 5.4 (assuming walls of boron-loaded concrete). As found for urine, lower radioactivity is observed with the boron addition in the walls material, and also in this case the most problematic activated isotope appears to be chlorine.

Nuclide	Half-life [s]	R [$s^{-1} g^{-1}$]	a [Bq/g]
Cl-38	37.24 min	34.98 ± 0.07	23.53 ± 0.04
K-42	12.360 h	30.80 ± 0.06	1.680 ± 0.003
Fe-59	44.503 d	0.4180 ± 0.0011	0.0002712 ± 0.000007

Table 5.3: Simulated reaction rates and specific activity after 2h of irradiation for soft tissue elements, with the walls of ordinary concrete

Nuclide	Half-life	R [$s^{-1} g^{-1}$]	a [Bq/g]
Cl-38	37.24 min	13.19 ± 0.04	8.88 ± 0.03
K-42	12.360 h	12.40 ± 0.04	0.676 ± 0.002
Fe-59	44.503 d	0.203 ± 0.001	0.0001317 ± 0.0000006

Table 5.4: Simulated reaction rates and specific activity after 2h of irradiation for soft tissue elements, with the walls of borated concrete

Conclusions and future studies

This thesis represents a preliminary evaluation of some radiation protection issues for the design of the BNCT clinical facility at CNAO *Phase II*, in particular concerning the project of the treatment rooms.

The first results obtained concerned the characterization of a new material, currently under test, as an optimal candidate to moderate the neutron beam. Aluminum fluoride has proven to be the best material to tailor a clinical neutron beam, and its solid form has been recently developed by sintering process. The first goal of this work was to study the activation of this material. Two kinds of powder were irradiated for neutron activation analysis, that allowed a quantification of trace elements. Moreover, dose was measured after irradiation as a function of the time. The results of the dosimetry and some considerations about the behaviour of the powders in the sinterization process allowed the selection of one type of powder as the most suitable for the construction of the Beam Shaping Assembly. The knowledge of the trace elements enabled the simulation of the BSA activation when installed in the beam.

The second part of the work concerned air activation, in particular, the production of argon 41 whose release in the environment could represent a problem due to radiation protection regulation. The effect of the material chosen as shieldings was studied by means of Monte Carlo simulations, leading to the choice of boron-loaded concrete as walls material. This configuration allows a residual activity in air lower than 1 Bq/g, which represents the established design goal. Different walls materials were tested also concerning the dosimetry in the room and the activation inside the walls, confirming that the best shielding is borated concrete. In order to investigate also the effects in the whole body of a patient, an anthropomorphic model was simulated in the clinical irradiation position, and the dose was calculated in the principal organs. Dosimetry and residual activity after 2 hours of treatment (a conservative value, considering that typical irradiation times in BNCT are of the order of 1 hour) were evaluated.

For the definitive design of the facility, every topic discussed in this work needs to be investigated in more detail. An important point is that all the elements necessary for the patient irradiation (supports and additional structures for patient positioning and immobilization, e.g. the treatment couch) need to be tested from the point of view of activation. Moreover, if any electronics will be present, its resistance to neutron irradiation must be studied.

With the prospect of a long-term use of the facility, a relevant aspect is to evaluate

the possible deterioration of the materials caused by exposure to radiations. This is of particular importance for AlF_3 in the BSA: if solid material loses consistency after exposures to high neutron fluence, volumes of lower density may appear and the spectrum of the neutron beam may be different than one expected. To this end, tests on solid AlF_3 are planned at the TRIGA reactor in Pavia, where the Central Thimble facility provides a very high neutron flux. With some hours of irradiation in the reactor, it is possible to reproduce long working time of the accelerator facility, thus is possible to perform mechanical tests of resistance.

Moreover, a secure stay in the room must be ensured, with a safe access to the structural components of the facility for any needed maintenance: the cumulative effect of neutron activation over several hours of beam working has to be assessed, so that no material present in the treatment room becomes excessively radioactive.

This thesis presents the results obtained by means of experimental measurements and simulations for the radioprotection assessment of the facility. When designing a neutron beam and the entire facility for BNCT, the work to optimize the dose delivery to the tumour, the calculation of the shielding to cut the dose outside the building and the study of residual activation of the materials are strictly interconnected. This thesis reports an example of this procedure, starting from a beam tailored for deep-seated tumours a preliminary design of the treatment room was obtained, considering the radiation protection prescriptions.

Bibliography

- [1] BARTH R.F., VICENTE M.G., HARLING O.K., KIGER W.S.III, RILEY K.J., BINNS P.J. ET AL., *Current status of Boron Neutron Capture Therapy of high grade gliomas and recurrent head and neck cancer* in "Radiation Oncology" 7(146):1-21, 2012
- [2] KREINER A.J., *Accelerator-based BNCT* in SAUERWEIN W.A.G, WITTIG A., MOSS R., NAKAGAWA Y. Editors "*Neutron Capture Therapy Principles and Applications*" Springer, 2012
- [3] ESPOSITO J., COLAUTTI P., FABRITISIEV S., GERVASH A., GINIYATULIN R., LOMASOV V.N., MAKHANKOV A., MAZUL I., PISENT A., POKROVSKY A., RUMYANTSEV M., TANCHUK V., TECCHIO L. , *Be target development for the accelerator-based SPES-BNCT facility at INFN Legnaro* in "Applied Radiation and Isotopes" 67(7-8 Suppl):S270-3, 2009
- [4] BORTOLUSSI S., POSTUMA I., PROTTI N., PROVENZANO L., FERRARI C., CAN-SOLINO L., DIONIGI P., GALASSO O., GASPARINI G., ALTIERI S., MIYATAKE S., GONZÁLEZ S.J., *Understanding the potentiality of accelerator based-boron neutron capture therapy for osteosarcoma: dosimetry assessment based on the reported clinical experience.* in "Radiation Oncology", 12(1):130, Aug 2017
- [5] FARÌAS R.O., BORTOLUSSI S., MENÉNDEZ P.R., GONZÁLEZ S., *Exploring boron neutron capture therapy for non-small cell lung cancer* in "Physica Medica", 30(8):888-897, Dec 2014
- [6] POSTUMA I., *Clinical application of accelerator-based Boron Neutron Capture Therapy: optimization of procedures, tailoring of a neutron beam and evaluation of its dosimetric performance.*, Ph.D. Thesis University of Pavia, 2015
- [7] MCNPTM-A General Monte Carlo N-Particle Transport Code, version 5, Technical report, LA-UR-03-1987 Los Alamos National Laboratory, 2003
- [8] INTERNATIONAL ATOMIC ENERGY AGENCY, *Reference neutron activation library*, IAEA-TECDOC-1285 IAEA Nuclear Data Section, 2002

- [9] INTERNATIONAL NUCLEAR DATA COMMITTEE, *Thermal neutron capture cross sections, resonance integrals and G-factors*, INDC(NDS)-440
IAEA Nuclear Data Section, 2003
- [10] LABORATORIO ENERGIA NUCLEARE APPLICATA, *Rapporto finale di sicurezza*,
Technical Report
LENA, 1999
- [11] AGOSTEO S., COLAUTTI P., ESPOSITO J., FAZZI A., INTROINI M.V., POLA A.,
Characterization of the energy distribution of neutrons generated by 5 MeV protons on a thick beryllium target at different emission angles
in "Applied Radiation and Isotopes" 69(12):1664-1667, 2011
- [12] GRUPEN C., *Introduction to Radiation Protection, practical knowledge for handling radioactive sources*
Springer, 2010
- [13] PELLICIONI M., *Fondamenti Fisici della Radioprotezione*
Pitagora Editrice Bologna, 1989
- [14] GOORLEY J.T., KIGER W.S. III, ZAMENHOF R.G., *Reference Dosimetry Calculations for Neutron Capture Therapy with Comparison of Analytical and Voxel Models*
in "Medical Physics", 29(2):145-56, Feb 2002
- [15] INTERNATIONAL COMMISSION ON RADIATION PROTECTION, *Conversion Coefficients for Radiological Protection Quantities for External Radiation Exposures*
ICRP Publication 116, Ann. ICRP 40(2-5), 2010
- [16] OBERHOFER M., *Advances in Radiation Protection*
Kluwer Academic Publishers, 1991
- [17] SHLEIEN B., *Health Physics and Radiological Health Handbook*, revised edition
Scinta inc., 1998
- [18] PELLICIONI M., FERRARI A. *Conversion Data and Effective Quality Factors for High-energy Neutrons*
Radiation Protection Dosimetry 76, 215-224, 1998
- [19] WOODWARD H.Q., WHITE D.R., *The composition of body tissues*
in "British Journal of Radiology", 59:1209-19, 1986